

Loop quantum cosmology of $k=1$ FRW models

Abhay Ashtekar^{1,2,*}, Tomasz Pawłowski^{1,†}, Parampreet Singh^{1,‡} and Kevin Vandersloot^{1,3§}

¹*Institute for Gravitational Physics and Geometry,
Physics Department, Penn State, University Park, PA 16802, U.S.A.*

²*Institute for Theoretical Physics, University of Utrecht,
Princetonplein 5, 3584 CC Utrecht, The Netherlands*

³*Institute of Cosmology and Gravitation, Mercantile House,
Portsmouth University, Portsmouth PO1 2EG, U.K.*

The closed, $k=1$, FRW model coupled to a massless scalar field is investigated in the framework of loop quantum cosmology using analytical and numerical methods. As in the $k=0$ case, the scalar field can be again used as emergent time to construct the physical Hilbert space and introduce Dirac observables. The resulting framework is then used to address a major challenge of quantum cosmology: resolving the big-bang singularity while retaining agreement with general relativity at large scales. It is shown that the framework fulfills this task. In particular, for states which are semi-classical at some late time, the big-bang is replaced by a quantum bounce and a recollapse occurs at the value of the scale factor predicted by classical general relativity. Thus, the ‘difficulties’ pointed out by Green and Unruh in the $k=1$ case do not arise in a more systematic treatment. As in $k=0$ models, quantum dynamics is deterministic across the deep Planck regime. However, because it also retains the classical recollapse, in contrast to the $k=0$ case one is now led to a cyclic model. Finally, we clarify some issues raised by Laguna’s recent work addressed to computational physicists.

PACS numbers: 04.60.Kz, 04.60Pp, 98.80Qc, 03.65.Sq

I. INTRODUCTION

The spatially flat, isotropic, $k=0$ model was recently investigated in detail in the setting of loop quantum cosmology (LQC) [1–3]. That investigation introduced a conceptual framework and analytical and numerical tools to construct the *physical sector* of the quantum theory. These methods enabled one to systematically explore the effects of quantum geometry both on the gravitational and matter sectors and to extend previous results in LQC. The purpose of this paper is to use the ‘improved dynamics’ of [3] to carry out a similar analysis for the closed, $k=1$ model, coupled to a massless scalar field. In our presentation, we will skip those constructions, proofs and arguments which are direct analogs of the ones used in the $k=0$ case in [1–3]. The focus will be on the differences from the existing treatments of

*Electronic address: ashtekar@gravity.psu.edu

†Electronic address: pawlowski@gravity.psu.edu

‡Electronic address: singh@gravity.psu.edu

§Electronic address: Kevin.Vandersloot@port.ac.uk

the $k=1$ model and also our earlier analysis of the $k=0$ model.

Although current observations favor spatially flat models, the $k=1$ closed model is of considerable conceptual and technical interest. On the conceptual side, an outstanding problem in quantum cosmology—and indeed in full quantum gravity—is whether one can construct a framework that cures the short-distance difficulties faced by the classical theory near singularities, while maintaining an agreement with it at large scales. By their very construction, perturbative and effective descriptions have no problem with the second requirement. However, physically their implications can not be trusted at the Planck scale and mathematically they generally fail to provide a deterministic evolution across the putative singularity. In loop quantum gravity (LQG) the situation is just the opposite. Quantum geometry gives rise to new discrete structures at the Planck scale that modify the classical theory in such a way that, at least in simple models, space-like singularities of general relativity are resolved. However, since the emphasis is on background independence and non-perturbative methods, a priori it is not clear whether the theory also has a rich semi-classical sector. Do the novel dynamical corrections unleashed by the underlying quantum geometry naturally fade away at macroscopic distances or do they have unforeseen implications that prevent the theory from reproducing general relativity at large scales? While there is recent progress which indicates that LQG does admit a viable semi-classical sector near Minkowski space-time [4], further evidence is needed in other contexts such as cosmological settings.

The ‘improved dynamics’ of [3] successfully addressed this issue in the $k=0$ case. However, because classical recollapse, the $k=1$ model provides a more stringent tests. In particular using numerical evolutions of equations used in the early LQC works [5], Green and Unruh [6] had concluded that there may be a key difficulty: the LQC evolution appeared not to reproduce the recollapse predicted by general relativity. Since curvatures at the epoch of the classical recollapse are very small, this feature appeared to indicate that LQC would deviate from general relativity in perfectly ordinary situations. Thus, although the LQC equations used in the Green-Unruh analysis did cure the ultraviolet difficulties by resolving the singularity in the sense of [7], they appeared not to have a viable infrared behavior. Can this difficulty be resolved? Or, does the situation in the $k=1$ model indicate that LQG may not admit a good semi-classical sector in this cosmological setting? We will employ methods developed in the $k=0$ case [3] to probe this issue in the *physical sector* of the quantum theory. A systematic analysis will show that not only is the big-bang singularity resolved but the quantum evolution in fact faithfully mirrors the predictions of general relativity, including the re-collapse, when the curvature is small compared to the Planck scale.

A second conceptual issue is whether the general features of the Planck scale physics found in the $k=0$ case in [3] are robust. For example, there the Friedmann equation $(\dot{a}/a)^2 = 8\pi G \rho/3$ is replaced in LQC by the quantum corrected equation $(\dot{a}/a)^2 = (8\pi G \rho/3)(1 - \rho/\rho_{\text{crit}})$ where $\rho_{\text{crit}} \approx 0.82\rho_{\text{Pl}}$. The correction comes with a negative sign, making it possible for \dot{a} to vanish—triggering a bounce—when the matter density reaches a critical value, ρ_{crit} . One then has a pre-big-bang branch joined on to the current post-big-bang branch by a deterministic evolution, both behaving classically when the density is low compared to ρ_{crit} . Does this feature survive in the $k=1$ case or does space-time simply become fuzzy near and to the ‘past’ of the big-bang? Is there only one cycle in which the universe resembles our own? Is the value of the critical density ρ_{max} at the bounce point essentially the same as in the $k=0$ model or does it depend on the spatial topology? Our analysis will show that the big-bang and the big-crunch are replaced by a quantum bounce leading, in a precise sense, to a cyclic quantum universe. Furthermore, the value of ρ_{max} is robust so long as the

maximum radius of the universe attains a macroscopic size.

On the technical side, this model also provides a number of challenges. In LQG, the configuration variable is a connection A_a^i , related to the spin connection Γ_a^i (determined by the spatial triad) and the extrinsic curvature K_a^i via $A_a^i = \Gamma_a^i + \gamma K_a^i$ where γ is the Barbero-Immirzi parameter. However, because of certain technical difficulties with the methods used, so far the $k=1$ case has been treated in the literature by regarding the extrinsic curvature K_a^i as a connection and constructing holonomies from it [5]. Because of gauge fixing this is a mathematically viable strategy. However as emphasized in, e.g. [6], to make closer contact with the full theory, it is desirable to construct the theory using connections A_a^i . So an important question arises: Can the improved dynamics of [3] overcome the difficulties faced in the earlier treatments, allowing us to formulate the theory in terms of A_a^i ? We will find that the answer is in the affirmative. A second technical challenge arises in the definition of the operator representing the field strength F_{ab}^i that features in the expression of the Hamiltonian constraint. In LQC, this operator is constructed from holonomies [8]. In the $k=0$ model, one can use the integral curves of the (right and left-invariant) fiducial triad ${}^0e_i^a$ to build the holonomy loops. In the $k=1$ case, ${}^0e_i^a$ (is only left invariant and) satisfies the commutation relations of $\mathfrak{so}(3)$. Hence none of the three pairs of triad vectors is surface forming. If one uses a general loop which is not tangential to these triads, holonomies (fail to be almost periodic functions of connections and) do not lead to well-defined operators in the quantum theory. Thus, finding suitable loops poses an interesting technical challenge. We resolve this issue.¹ Finally, to numerically solve the quantum Hamiltonian constraint, one has to find normalizable eigenfunctions of a certain difference operator Θ . Recall that in the case of, e.g., a simple harmonic oscillator, the differential operator representing the Hamiltonian admits an eigenfunction with any real number as its eigenvalue. Normalizable eigenfunctions exist only for discrete eigenvalues and thus constitute a set of zero measure in the space of all eigenfunctions. In the $k=1$ case, the situation is similar with the operator Θ . However, now the normalizable eigenfunctions and their eigenvalues are not known analytically and, since they constitute a set of zero measure, one has to exercise considerable care in singling them out numerically.

Insights gained from the resolution of these conceptual and technical issues are likely to be important as one considers more and more general situations and develop new tools to tackle the Hamiltonian constraint of full LQG.

The paper is organized as follows. In section II we summarize the basics of the classical and quantum theories for our model, arriving at the form of the Hamiltonian constraint operator. In section III we sketch the Wheeler-DeWitt (WDW) theory and in IV we introduce the physical sector of the theory in LQC. Numerical simulations are discussed in section V. In section VI we summarize effective equations of the semi-classical sector, list the main numerical results and compare them with predictions of the effective theory. We also clarify some issues that have been raised by a numerical analysis by Laguna [11] and remove confusion caused by an unfortunate use of terminology there. Section VII places these results in a broader context and discusses their relation with that by Green and Unruh [6]. Appendix A summarizes some background material on the fiducial geometrical structures used in $k=1$ models with the so-called ‘Bianchi IX’ symmetries.

¹ This issue was resolved independently by the Warsaw group [10]. Their method of evaluating the holonomy is more intrinsic, elegant and insightful.

II. THE BASIC FRAMEWORK

This section is divided into two parts. In the first we summarize the classical theory and in the second we present the basics of the quantum theory.

A. Classical Theory

Space-time manifolds under consideration are of the form $M \times \mathbb{R}$, where M has the topology of a 3-sphere, \mathbb{S}^3 . As explained in appendix A, one can identify M with the symmetry group $SU(2)$ (which ensures spatial homogeneity and isotropy) and endow it with a fixed fiducial basis of 1-forms ${}^o\omega_a^i$ and vectors ${}^oe_i^a$. The resulting fiducial metric is

$${}^oq_{ab} := {}^o\omega_a^i {}^o\omega_b^j k_{ij}, \quad k_{ij}: \text{ the Cartan-Killing metric on } \mathfrak{su}(2). \quad (2.1)$$

${}^oq_{ab}$ turns out to be the metric of the round 3-sphere with radius $a_o = 2$ (rather than $a_o = 1$). The volume of M w.r.t. this fiducial metric ${}^oq_{ab}$ is $V_o = 2\pi^2 a_o^3 = 16\pi^2$ and the scalar curvature is ${}^oR = 6/a_o^2 = 3/2$. We shall set $\ell_o := V_o^{1/3}$. (For details, see Appendix A).

To facilitate comparison with the spatially flat, $k=0$ case and to directly use results of [1–3] obtained in that case, we will set our conventions in a parallel fashion. The dynamical, isotropic homogeneous connections and triads will be parameterized by c and p respectively:

$$A_a^i = c \ell_o^{-1} {}^o\omega_a^i, \quad E_i^a = p \ell_o^{-2} \sqrt{{}^oq} {}^oe_i^a. \quad (2.2)$$

As in the $k=0$ case c is dimensionless while p has dimensions of area and the density weight of E_i^a is absorbed in the determinant of the fiducial metric. At the point (c, p) of the phase space, the physical 3-metric q_{ab} and the extrinsic curvature K_{ab} are given by:

$$q_{ab} = |p| \ell_o^{-2} {}^oq_{ab} \quad \text{and} \quad \gamma K_{ab} = (c - \frac{\ell_o}{2}) |p|^{\frac{1}{2}} \ell_o^{-2} {}^oq_{ab} \quad (2.3)$$

The corresponding physical volume of M is $|p|^{\frac{3}{2}}$. The scale factor a associated with a physical metric q_{ab} is generally expressed via $q_{ab} = a^2 {}^oq_{ab}$ where ${}^oq_{ab}$ is the *unit* 3-sphere metric. Then, the scale factor is related to p via $|p| = a^2 \ell_o^2 / 4$. As usual p can take both positive and negative values, the change in sign corresponds to a flip in the orientation of the triads ${}^oe_i^a$ which leaves the physical metric q_{ab} invariant.

Expressions of the total action, the symplectic structure, and the Hamiltonian constraint require an integration over M . In the $k=0$ case the underlying manifold is non-compact (\mathbb{R}^3), whence the naive integrals would simply diverge. Therefore, irrespective of which quantization scheme one uses, one has to fix a fiducial cell with finite volume, say \mathcal{V}_o (w.r.t. the fiducial flat metric), and restrict all integrations to this cell. In the $k=1$ case, M is compact and the introduction of a cell is unnecessary. Nonetheless, in many of the key equations our V_o plays the role of the volume \mathcal{V}_o of the cell in the $k=0$ case. In both cases, the fundamental Poisson bracket is:

$$\{c, p\} = \frac{8\pi G\gamma}{3} \quad (2.4)$$

where γ is the Barbero-Immirzi parameter. Finally, using the fact that the Cartan orthonor-

mal triad ω_a^i on a 3-sphere of radius a_o satisfies the identity

$$d\omega^k + \frac{1}{a_o} \epsilon_{ij}{}^k \omega^i \wedge \omega^j = 0, \quad (2.5)$$

it is straightforward to calculate the field strength F_{ab}^k of the connection A_a^i on M

$$F_{ab}^k = \ell_o^{-2} \left[c^2 - c \ell_o \left(\frac{2}{a_o} \right) \right] \epsilon_{ij}{}^k \omega_a^j \omega_b^i. \quad (2.6)$$

Our fiducial co-triad ω_a^i corresponds to $a_o = 2$. But we have refrained from using this numerical value in (2.6) to clarify the relation with the $k=0$ case. To pass to this case, one has to set V_o equal to the volume \mathcal{V}_o of the fiducial cell there but take the limit as a_o goes to infinity. In this limit, the fiducial co-triad ω_a^i goes to the (flat) fiducial co-triad used in the $k=0$ case (see (2.5)) and the field strength F_{ab}^k goes over to its value $\mathcal{V}_o^{-2/3} c^2 \epsilon_{ij}{}^k \omega_a^j \omega_b^i$ in the $k=0$ case [1–3, 8].

As in the $k=0$ models, we have completely gauge fixed the Gauss and the diffeomorphism constraints by fixing ω_a^i and e_i^a and using the parametrization (2.2) of the phase space variables A_a^i, E_i^a . So, we are left only with the Hamiltonian constraint. The gravitational part of this constraint is given by [12, 15]:

$$C_{\text{grav}} = \int_M d^3x \left[\epsilon^{ij}{}_k e^{-1} E^{ai} E^{bj} F_{ab}^k - 2(1 + \gamma^2) e^{-1} E^{ai} E^{bj} K_{[a}^i K_{b]}^j \right], \quad (2.7)$$

where $e := \sqrt{|\det E|}$ and $K_a^i = K_a{}^b \omega_b^i$ is the extrinsic curvature, and where, as is usual in mini-superspace analysis, we have set the lapse equal to 1. Using the fact that A_a^i is related to the spin-connection Γ_a^i (of the physical triad e_i^a) and the extrinsic curvature K_a^i through $A_a^i = \Gamma_a^i + \gamma K_a^i$, it is convenient to express the second term in the integrand of (2.7) in terms of the curvature F_{ab}^k of A_a^i and the curvature Ω_{ab}^k of Γ_a^i :

$$E^{ai} E^{bj} K_{[a}^i K_{b]}^j = \frac{1}{2\gamma^2} \epsilon^{ij}{}_k E^{ai} E^{bj} (F_{ab}^k - \Omega_{ab}^k). \quad (2.8)$$

In the $k=0$ case, the spatial curvature Ω_{ab}^k vanishes and the extrinsic curvature term in (2.7) reduces to a multiple of the first term involving F_{ab}^k . In full general relativity, by contrast, while Ω_{ab}^i is determined by the momenta E_i^a , its expression is rather complicated and this strategy of handling the extrinsic curvature terms, by itself, does not simplify matters. The situation in general homogeneous models [5] as well as black hole interiors [13] is in between the two: Although Ω_{ab}^k is non-zero, its expression is simple and manageable. In the $k=1$ model now under consideration one has:

$$\Omega_{ab}^k = -\frac{1}{4} \epsilon_{ij}{}^k \omega_a^i \omega_b^j. \quad (2.9)$$

Therefore, the gravitational part of the constraint reduces to:

$$C_{\text{grav}} = -\frac{1}{\gamma^2} \int_M d^3x \epsilon^{ij}_k e^{-1} E^a_i E^b_j \left[F^k_{ab} - \left(\frac{1+\gamma^2}{4} \right) {}^o\epsilon_{ab}{}^c {}^o\omega_c^k \right] \quad (2.10)$$

$$= -\frac{6\sqrt{p}}{\gamma^2} \left[\left(c - \frac{\ell_o}{2} \frac{2}{a_o} \right)^2 + \frac{\gamma^2 \ell_o^2}{4} \frac{4}{a_o^2} \right] \quad (2.11)$$

where, in the last step we have used the expression (2.6) of F_{ab} . In the $k=1$ case now under consideration, $a_o = 2$. However, as indicated above, we did not substitute this numerical value because results for the $k=0$ case [1–3] can be recovered by setting $a_o = \infty$ (and $\ell_o = \mathcal{V}_o^{1/3}$). However, since a_o always occurs in the combination ℓ_o/a_o in the Hamiltonian constraint, we can set $a_o = 2$ throughout and recover the $k=0$ results simply by setting $\ell_o = 0$. In what follows, we will adopt this strategy.

Remark: In the above construction, we began with a fiducial triad ${}^oe_i^a$ and a co-triad ${}^o\omega_a^i$ adapted to a 3-sphere of radius $a_o=2$. Therefore, our construction may appear to be tied to that choice. Had we used a 3-sphere of radius $a_o = 2\lambda$, the fiducial triad and the co-triad we have rescaled via ${}^oe_i^a \rightarrow \lambda^{-1} {}^o\omega_a^i$ and ${}^o\omega_a^i \rightarrow \lambda {}^o\omega_a^i$. It is easy to check that the variables c, p parameterizing the physical fields (A_a^i, E_i^a) are left unchanged. Hence the entire framework is invariant under this rescaling ‘gauge’ freedom.

B. Quantum kinematics and the Hamiltonian constraint

To pass to the quantum theory, following Dirac one first constructs a kinematical description. As in the $k=0$ case [1–3, 8] the kinematical Hilbert space $\mathcal{H}_{\text{kin}}^{\text{grav}}$ is the space $L^2(\mathbb{R}_{\text{Bohr}}, d\mu_{\text{Bohr}})$ of square integrable functions on the Bohr compactification of the real line. To specify states concretely, it is convenient to work with the representation in which the operator \hat{p} is diagonal. Eigenstates of \hat{p} are labeled by a real number μ and satisfy the orthonormality relation:

$$\langle \mu_1 | \mu_2 \rangle = \delta_{\mu_1, \mu_2} . \quad (2.12)$$

Since the right side is the Kronecker delta rather than the Dirac delta distribution, a typical state in $\mathcal{H}_{\text{kin}}^{\text{grav}}$ can be expressed as a countable sum; $|\Psi\rangle = \sum_n c^{(n)} |\mu_n\rangle$ where $c^{(n)}$ are complex coefficients and the inner product is given by

$$\langle \Psi_1 | \Psi_2 \rangle = \sum_n \bar{c}_1^{(n)} c_2^{(n)} . \quad (2.13)$$

The fundamental operators are \hat{p} and $\widehat{\exp i\lambda(c/2)}$:

$$\hat{p} |\mu\rangle = \frac{8\pi\gamma\ell_{\text{Pl}}^2}{6} \mu |\mu\rangle \quad \text{and} \quad \widehat{\exp \frac{i\lambda c}{2}} |\mu\rangle = |\mu + \lambda\rangle \quad (2.14)$$

where λ is any real number. From the discussion of the classical theory of section II A it follows that the physical volume operator of M is given by: $\hat{V} = |\hat{p}|^{3/2}$.

Of special interest to us are holonomies of the connection A_a^i along the integral curves of our fiducial triads ${}^oe_i^a$. The holonomy $h_k^{(\lambda)}$ along the segment of (directed) length $\lambda\ell_o$,

tangential to e_k^a is given by:²

$$h_k^{(\lambda)} = \cos \frac{\lambda c}{2} \mathbb{I} + 2 \sin \frac{\lambda c}{2} \tau_k. \quad (2.15)$$

The corresponding holonomy operator has the action:

$$\hat{h}_k^{(\lambda)} |\mu\rangle = \frac{1}{2} (|\mu + \lambda\rangle + |\mu - \lambda\rangle) \mathbb{I} + \frac{1}{i} (|\mu + \lambda\rangle - |\mu - \lambda\rangle) \tau_k. \quad (2.16)$$

However, just as there is no operator corresponding to the connection itself in full LQG [12, 15], there is no operator \hat{c} on $\mathcal{H}_{\text{kin}}^{\text{grav}}$ [8].

To describe quantum dynamics, we have to first introduce a well-defined operator on $\mathcal{H}_{\text{kin}}^{\text{grav}}$ representing the Hamiltonian constraint C_{grav} . Since there is no operator corresponding to c itself, as in the $k=0$ case we will use the integral expression (2.10) of the constraint. For the passage to quantum theory, one has to first express this classical constraint in terms of the elementary variables p and $h_k^{(\lambda)}$ and then replace them with operators \hat{p} and $\hat{h}_k^{(\lambda)}$. As in the full theory [14, 15], the term involving triads becomes the following operator [2, 3, 8]

$$\epsilon_{ijk} e^{-1} \widehat{E^{aj} E^{bk}} = \sum_k \frac{(\text{sgn } p)}{2i\hbar \pi \gamma G \lambda \ell_o} \epsilon^{abc} \omega_c^k \text{Tr} \left(\hat{h}_k^{(\lambda)} [\hat{h}_k^{(\lambda)-1}, \hat{V}] \tau_i \right) \quad (2.17)$$

where $\hat{V} = |\hat{p}|^{3/2}$ is the volume operator.

To define \hat{F}_{ab}^k in (2.10), as in [1–3, 8] we use the standard relation between the holonomies and field strengths. Because of homogeneity, the components $\mathcal{e}_i^a \mathcal{e}_j^b F_{ab}^k$ are constant on M . They can be evaluated by considering a square loop \square_{ij} starting and ending at any point x , with tangent vectors \mathcal{e}_i^a and \mathcal{e}_j^b at x , and then taking the limit as the area enclosed by the loop shrinks to zero. In the quantum theory, since there is no operator corresponding to the connection c , the limiting operator does not exist. As discussed in detail in [1–3, 8], this is a manifestation of the quantum nature of geometry, i.e., a reflection of the fact that the area operator has purely discrete spectrum. As in [3] our strategy is to shrink the loop only until its *physical* area equals the ‘area gap’ Δ , i.e., the minimal non-zero eigenvalue of the area operator.

Now, in the $k=0$ case, the edges of \square_{ij} can be taken to be the integral curves of the triad vector fields \mathcal{e}_i^a and \mathcal{e}_j^b . In the $k=1$ model, however, the \mathcal{e}_i^a satisfy the commutation relations of $\mathfrak{su}(2)$; they do not commute. Therefore their integral curves can not provide the desired closed loop \square_{ij} . In the existing literature, a closed loop is formed by simply adding a fifth edge [5]. However, this strategy is not viable: Since the five edges do not span an unambiguous 2-surface, the notion of the area enclosed by the loop has no obvious meaning. However, note that while \mathcal{e}_i^a are the ‘left-invariant’ vector fields, M also admits three ‘right invariant’ vector fields ξ_i^a (see Appendix A). These are the symmetry fields: they also satisfy the commutation relations of $\mathfrak{su}(2)$, act simply and transitively on M and their action leaves each of our fiducial triads \mathcal{e}_i^a and co-triads ω_a^i invariant. Since they commute with \mathcal{e}_i^a , one

² Here \mathbb{I} is the unit 2×2 matrix and τ_k is a basis in the Lie algebra $\mathfrak{su}(2)$ satisfying $\tau_i \tau_j = \frac{1}{2} \epsilon_{ijk} \tau^k - \frac{1}{4} \delta_{ij}$. Thus, $2i\tau_k = \sigma_k$, where σ_i are the Pauli matrices. The directed length is positive if the line segment is oriented along \mathcal{e}_k^a and negative if it is oriented in the opposite direction.

can form the desired closed loops \square_{ij} by first moving from x along the integral curve of say ${}^o e_i$ then ξ_k then along $-{}^o e_i$ and then along $-\xi_k$ (where ξ_k is chosen to coincide with ${}^o e_j$ at x). An explicit realization of this procedure is presented in Appendix A and a more geometric construction appears in [10]. The final field strength operator does not depend on whether the first segment is chosen to be left invariant or right invariant and is given by³:

$$\begin{aligned}\hat{F}_{ab}^k &= \lim_{Ar \square_{ij} \rightarrow \Delta} \frac{1}{\lambda^2 \ell_o^2} \left(\sin^2 \lambda(c - \ell_o/2) - \sin^2(\lambda \ell_o/2) \right) \epsilon_{ij}{}^k {}^o \omega_a^i {}^o \omega_b^j \\ &= \frac{1}{\bar{\mu} \ell_o^2} \left(\sin^2 \bar{\mu}(c - \ell_o/2) - \sin^2(\bar{\mu} \ell_o/2) \right) \epsilon_{ij}{}^k {}^o \omega_a^i {}^o \omega_b^j.\end{aligned}\quad (2.18)$$

Here, as discussed in detail in [3], $\bar{\mu}$ is a specific function of p :

$$\bar{\mu}^2 |p| = \Delta \equiv (2\sqrt{3}\pi\gamma) \ell_{\text{Pl}}^2, \quad (2.19)$$

and for notational simplicity we have dropped hats on operators which are trigonometric functions of c . The fact that $\bar{\mu}$ is a function of p rather than a constant arises from the requirement that the *physical* area of \square_{ij} be set equal to Δ . As explained in [3], this strategy mimics the full theory in a well-defined sense and the resulting ‘improved dynamics’ is free of the drawbacks of older Hamiltonian constraint of LQC. As in [1–3, 8], the viewpoint is that at the fundamental level —i.e. at the Planck scale— the field strength operator is non-local and the usual local classical expression arises only on coarse graining in semi-classical states.

To obtain the explicit action of \hat{F}_{ab}^k on $\mathcal{H}_{\text{kin}}^{\text{grav}}$, one has to face two complications. The first arises already in the $k=0$ case. The operator \hat{F}_{ab}^k for $k=0$ can be recovered by setting $\ell_o = 0$. It depends on the connection only through $\sin(\bar{\mu}c)$. Since $\bar{\mu}$ is itself a function of \hat{p} , the action of $\sin \bar{\mu}c$ on $\mathcal{H}_{\text{kin}}^{\text{grav}}$ is rather subtle. As discussed in detail in [3], it is simplest to express it by going to a basis $|v\rangle$ which is better adapted to the volume operator \hat{V} :

$$\hat{V}|v\rangle = \left(\frac{8\pi\gamma}{6}\right)^{\frac{3}{2}} \frac{|v|}{K} \ell_{\text{Pl}}^3 |v\rangle \quad (2.20)$$

where the dimensionless label v —the eigenvalue of \hat{V} apart from a constant— is related to the dimensionless label μ —the eigenvalue of \hat{p} apart from an overall constant— via

$$v = K \text{sgn}(\mu) |\mu|^{\frac{3}{2}}, \quad \text{where} \quad K = \frac{2\sqrt{2}}{3\sqrt{3\sqrt{3}}}. \quad (2.21)$$

In this basis, $\exp i\bar{\mu}c$ are simply the translation operators:

$$e^{i\frac{\bar{\mu}c}{2}} \Psi(v) = \Psi(v+1), \quad (2.22)$$

so that

$$\sin(\bar{\mu}c) \Psi(v) = \frac{1}{2i} (\Psi(v+2) - \Psi(v-2)). \quad (2.23)$$

³ Here and in what follows, in light of results of [16, 17], we have used the fundamental, $j = 1/2$ representation. For a more detailed discussion, see [2, 3].

In the $k=1$ case we have an added complication: (2.18) contains $\sin \bar{\mu}(c - \ell_o/2)$ rather than $\sin(\bar{\mu}c)$. This difference can be handled as follows: On $\mathcal{H}_{\text{kin}}^{\text{grav}}$

$$\sin(\bar{\mu}c - \frac{\ell_o}{2}) \Psi(v) = e^{i\ell_o f} \sin \bar{\mu}c e^{-i\ell_o f} \Psi(v), \quad \text{where} \quad f = \frac{\text{sgn } v}{4} \left| \frac{v}{K} \right|^{\frac{2}{3}}. \quad (2.24)$$

Note that since $f(v)$ is continuous everywhere (including the point $v = 0$), the operator $\exp i\ell_o f$ is well-defined and unitary on all of $\mathcal{H}_{\text{kin}}^{\text{grav}}$.

We now have operators corresponding to each term in the integrand of the gravitational part (2.10) of the Hamiltonian constraint. Using (2.17), (2.18), (2.23) and (2.24) in (2.10) we obtain:

$$\begin{aligned} \hat{C}_{\text{grav}} \Psi(v) = & e^{if\ell_o} \sin \bar{\mu}c \hat{A} \sin \bar{\mu}c e^{-i\ell_o f} \Psi(v) \\ & - \left[\sin^2 \frac{\bar{\mu}\ell_o}{2} - \frac{\bar{\mu}^2 \ell_o^2}{4} - \frac{\ell_o^2}{9|K^2 v|^{\frac{2}{3}}} \right] \hat{A} \Psi(v) \end{aligned} \quad (2.25)$$

where, as in the $k=0$ analysis [3] we have set

$$\hat{A} \Psi(v) = -\frac{27K}{4} \sqrt{\frac{8\pi}{6}} \frac{\ell_{\text{Pl}}}{\gamma^{3/2}} |v| \left| |v-1| - |v+1| \right| \Psi(v). \quad (2.26)$$

To summarize, there are two main subtleties in the passage from spatially flat, $k=0$ models to the closed, $k=1$ ones. First, the loop around which holonomy is computed has to be constructed using both right and left invariant vector fields. Second, now the connection dependence is in the operator $\sin \bar{\mu}(c - \ell_o/2)$ rather than $\sin \bar{\mu}c$ and one has to define its action on $\mathcal{H}_{\text{kin}}^{\text{grav}}$ using the unitary operators $\exp i\ell_o f$. When this is done, the gravitational part of the Hamiltonian constraint is symmetric and positive, given by (2.25).

Finally, to write the complete constraint operator we also need the matter part of the constraint. For the massless scalar field, in the classical theory it is given by:

$$C_{\text{matt}} = 8\pi G |p|^{-\frac{3}{2}} p_\phi^2 \quad (2.27)$$

As usual, the non-trivial part in the passage to quantum theory is the function $|p|^{-3/2}$. However, as with the co-triad operator (2.17), we can use the method introduced by Thiemann in the full theory [14, 15]. This issue is discussed in detail in [3]. The final result is:

$$\widehat{|p|^{-\frac{3}{2}}} \Psi(v) = \left(\frac{6}{8\pi\gamma\ell_{\text{Pl}}^2} \right)^{3/2} B(v) \Psi(v) \quad (2.28)$$

where

$$B(v) = \left(\frac{3}{2} \right)^3 K |v| \left| |v+1|^{1/3} - |v-1|^{1/3} \right|^3. \quad (2.29)$$

It is self-adjoint on $\mathcal{H}_{\text{kin}}^{\text{grav}}$ and diagonal in the eigenstates of the volume operator.

Collecting these results we can express the total constraint

$$\hat{C} \Psi(v) = \left(\hat{C}_{\text{grav}} + \hat{C}_{\text{matt}} \right) \Psi(v) = 0, \quad (2.30)$$

as follows:

$$\begin{aligned}
\partial_\phi^2 \Psi(v, \phi) &= - \Theta \Psi(v, \phi) \\
&= - \Theta_o \Psi(v, \phi) + \frac{\pi G}{2} [B(v)]^{-1} \left[3K(\sin^2(\frac{\bar{\mu} \ell_o}{2}) - \frac{\bar{\mu}^2 \ell_o^2}{4}) |v| \right. \\
&\quad \left. - \frac{1}{3} \ell_o^2 \gamma^2 \left| \frac{v}{K} \right|^{\frac{1}{3}} \right] \left[|v-1| - |v+1| \right] \Psi(v, \phi).
\end{aligned} \tag{2.31}$$

Here, Θ_o is the operator that appears in the $k=0$ quantum constraint in place of Θ [3]:

$$\Theta_o \Psi(v, \phi) = -[B(v)]^{-1} (C^+(v) \Psi(v+4, \phi) + C^o(v) \Psi(v, \phi) + C^-(v) \Psi(v-4, \phi)) \tag{2.32}$$

where the coefficients $C^\pm(v)$ and $C^o(V)$ are given by:

$$\begin{aligned}
C^+(v) &= \frac{3\pi KG}{8} |v+2| \left| |v+1| - |v+3| \right| \\
C^-(v) &= C^+(v-4) \\
C^o(v) &= -C^+(v) - C^-(v).
\end{aligned} \tag{2.33}$$

Thus, the $k=1$ quantum constraint has the same form as in the $k=0$ case. As one would expect from the classical expression (2.10), the difference $\Theta - \Theta_o$ is diagonal in the v -representation and vanishes when we set $\ell_o = 0$.

In the remainder of the paper, we will work with the Hamiltonian constraint (2.31). As in the $k=0$ case [2, 3], the form of this constraint is similar to that of a massless Klein-Gordon field in a static space-time, but now with an additional static potential. ϕ is the analog of the static time coordinate and the difference operator Θ , of the spatial Laplace-type operator plus the static potential. Hence, the scalar field ϕ can again be used as ‘emergent time’ in the quantum theory. We will examine the operator Θ in some detail in sections IV and V. Finally, in the above construction we made a factor ordering choice the motivations behind which are the same as those discussed in [3]. This choice will facilitate comparison between the LQC results in the $k=1$ and $k=0$ cases and yield the WDW equation with its ‘natural’ factor ordering in the ‘continuum limit’.

Remark: Velhinho [18] has pointed out that in quantum kinematics it would suffice to consider the algebra generated by p and just two almost periodic functions of the connection, $e^{i\mu_1 c}$ and $e^{i\mu_2 c}$, where μ_1/μ_2 is irrational, because these functions already separate points of the phase space. In the older, ‘ μ_o -evolution’ [2, 8], this strategy would be natural; one could set $\mu_1 = 1$ and $\mu_2 = \mu_o \equiv 3\sqrt{3}/2$. However, as discussed in [2], this evolution is not viable physically. The ‘improved’ $\bar{\mu}$ -evolution used in [3] and in this paper is free of those drawbacks. But since $\bar{\mu}$ is now not a constant but a function (2.19) of μ , the Velhinho kinematics will not support the ‘improved quantum dynamics.’

III. WHEELER DEWITT THEORY

In this section we will briefly discuss the WDW limit of LQC in which effects specific to quantum geometry in the difference equation (2.31) are ignored by letting the area gap go to zero. This discussion will bring out the key role played by quantum geometry near the big bang and the big crunch singularities. The WDW theory has its roots in geometrodynamics

which is insensitive to the choice of the triad orientation —i.e., to the sign of v . Therefore, as in [2, 3], we will restrict ourselves to wave functions $\underline{\Psi}(v)$ which are symmetric under the orientation reversal operator Π ,

$$\Pi \underline{\Psi}(v, \phi) = \underline{\Psi}(-v, \phi). \quad (3.1)$$

where (and in what follows) we have denoted the WDW analogs of the LQC quantities with an underbar. As in [3] we will find that the scalar field ϕ can again be used as emergent time and, in the resulting physical sector of the theory, the big bang and the big crunch singularities persist in the WDW limit. Details of motivation and background material as well as underlying assumptions and technical steps involved in the WDW limit can be found in [3].

A. The WDW constraint and its general solution

To pass to the WDW theory, one sends the area gap to zero and restricts oneself to *smooth* wave functions $\underline{\Psi}(v, \phi)$. As explained in [2, 3], this corresponds to taking the continuum limit of the difference equation (2.31). The non-trivial part of the task lies in the limit of Θ_o since the remainder is diagonal in v . This has already been completed in [3]. The required WDW limit is then given by⁴

$$\begin{aligned} \partial_\phi^2 \underline{\Psi}(v, \phi) &= -\underline{\Theta} \underline{\Psi}(v, \phi) \\ &= -\underline{\Theta}_o \underline{\Psi}(v, \phi) - \frac{\pi G \ell_o^2 \gamma^2}{3K^{\frac{4}{3}}} |v|^{\frac{4}{3}} \underline{\Psi}(v, \phi), \end{aligned} \quad (3.2)$$

where, as in [3],

$$\underline{\Theta}_o \underline{\Psi}(v, \phi) := -12\pi G (v \partial_v)^2 \underline{\Psi}(v, \phi). \quad (3.3)$$

As explained in [3], this factor ordering is ‘covariant’ from the geometrodynamical perspective and coincides with the one used in the older WDW literature (see e.g. [19]).

The operator $\underline{\Theta}$ is self-adjoint and positive definite on the Hilbert space $L^2(\mathbb{R}, \underline{B}(v) dv) \equiv L^2(\mathbb{R}, (K/|v|) dv)$, where, as in [3], to facilitate comparison with LQC results we have denoted the WDW limit $K/|v|$ of $B(v)$ by $\underline{B}(v)$. The general solution of (3.2) can be readily expressed in terms of the spectral family of $\underline{\Theta}$. Let us begin by considering all eigenfunctions of the differential operator $\underline{\Theta}$:

$$-12\pi G (v \partial_v)^2 \psi_\omega(v) + \frac{\pi G \ell_o^2 \gamma^2}{3K^{\frac{4}{3}}} |v|^{\frac{4}{3}} \psi_\omega(v) = \omega^2 \psi_\omega(v). \quad (3.4)$$

In their most general form, they can be expressed as linear combinations of modified Bessel

⁴ The appearance of the Barbero-Immirzi parameter γ in the WDW limit is an artifact of our conventions, i.e., definition of v . If instead we use the eigenvalue \bar{v} of the volume operator, $\hat{V}|\bar{v}\rangle = \bar{v} \ell_{\text{Pl}}^3 |\bar{v}\rangle$, so that $\bar{v} = (8\pi\gamma/6)^{\frac{3}{2}} (v/K)$, the WDW equation (3.2) would be manifestly independent of γ : $\partial_\phi^2 \underline{\Psi}(\bar{v}, \phi) = 12\pi G (\bar{v} \partial_{\bar{v}})^2 \underline{\Psi}(\bar{v}, \phi) - (G \ell_o^2 / 16\pi) \bar{v}^{4/3} \underline{\Psi}(\bar{v}, \phi)$.

functions \mathcal{I}, \mathcal{K} [19]

$$\psi_\omega(v) = \alpha \mathcal{K}_{ik} \left(\frac{\ell_o \gamma}{4K^{\frac{2}{3}}} |v|^{\frac{2}{3}} \right) + \beta \mathcal{I}_{ik} \left(\frac{\ell_o \gamma}{4K^{\frac{2}{3}}} |v|^{\frac{2}{3}} \right), \quad (3.5)$$

where $k := (3/16\pi G)^{\frac{1}{2}} \omega$ and α, β are constants. (We have used calligraphic letters to denote the modified Bessel functions to avoid confusion with the constant K of (2.21)). As $x \rightarrow \infty$, the function $\mathcal{I}_{ik}(x)$ grows exponentially whereas $\mathcal{K}_{ik}(x)$ decays exponentially.

These properties of eigenfunctions imply that the spectrum of the operator $\underline{\Theta}$ is continuous and that $\mathcal{I}_{ik}(x)$ cannot feature in its spectral decomposition. Therefore to obtain this decomposition, we will set $\beta(k) = 0$ and choose constants $\alpha(k)$ such that the resulting eigenfunctions $\underline{e}_k(v) := \alpha(k) \mathcal{K}_{ik}(v)$ are orthonormal,

$$\langle \underline{e}_k | \underline{e}_{k'} \rangle = \delta(k, k'). \quad (3.6)$$

The Dirac distribution appears on the right hand side because the spectrum of Θ is continuous. This may appear surprising because $\underline{e}_k(v)$ decay for large v . However, $\underline{e}_k(v)$ fail to have finite norm in $L^2(\mathbb{R}, (K/|v|)dv)$ because they have the following oscillatory form for small v

$$\mathcal{K}_{ik} \left(\frac{\ell_o \gamma}{4K^{\frac{2}{3}}} |v|^{\frac{2}{3}} \right) \xrightarrow{|v| \ll k} a(\omega) \cos \left(\frac{\omega}{\sqrt{12\pi G}} \ln |v| + \sigma(\omega) \right), \quad (3.7)$$

where $\sigma(\omega)$ is a constant (but ω -dependent) phase shift.

In the spatially open, $k=0$ models [3], the spectrum of $\underline{\Theta}$ is 2-fold degenerate, reflecting the fact that in the classical theory there are two sets of distinct solutions, one perpetually expanding and the other perpetually contracting. In the present case, this degeneracy is broken because $\mathcal{I}_{ik}(v)$ diverge at large v . Its classical counterpart is the fact that, because each solution has both contracting and expanding epochs, we no longer have two distinct sets of universes.

Eigenfunctions $\underline{e}_k(v)$ provide the standard spectral decomposition on $L^2(\mathbb{R}, \underline{B}(v)dv)$:

$$\underline{\Psi}(v) = \int_0^\infty dk \tilde{\Psi}(k) \underline{e}_k(v). \quad (3.8)$$

Hence, the general solution to (3.2) with smooth initial data consisting of rapidly decreasing functions can be written as

$$\underline{\Psi}(v, \phi) = \int_0^\infty dk \tilde{\Psi}_+(k) \underline{e}_k(v) e^{i\omega\phi} + \tilde{\Psi}_-(k) \underline{e}_k(v) e^{-i\omega\phi} \quad (3.9)$$

for some suitably regular function $\tilde{\Psi}_\pm(k)$. Following the terminology generally used in the Klein-Gordon theory, the solution will be said to be of positive (resp. negative) frequency if $\tilde{\Psi}_-(k)$ (resp. $\tilde{\Psi}_+(k)$) vanishes.

As usual, the positive and negative frequency solutions satisfy first order ‘evolution’ equations, obtained by taking a square-root of the constraint (3.2):

$$\mp i \partial_\phi \underline{\Psi}(v, \phi) = \sqrt{\underline{\Theta}} \underline{\Psi}(v, \phi). \quad (3.10)$$

If $f(v)$ is the initial data for these equations at ‘time $\phi = \phi_o$ ’, the solutions are given by:

$$\underline{\Psi}_{\pm}(v, \phi) = e^{\pm i \sqrt{\Theta} (\phi - \phi_o)} f(v). \quad (3.11)$$

B. Physical sector of the WDW theory

Solutions (3.9) to the WDW equation are not normalizable in $\mathcal{H}_{\text{kin}}^{\text{wdw}}$ (because zero is in the continuous part of the spectrum of the WDW operator). Therefore, one has to use one of the standard methods [20, 21] to construct the physical Hilbert space $\mathcal{H}_{\text{phy}}^{\text{wdw}}$. Since the procedure is completely analogous to that used in [2, 3], we will simply summarize the final results.

$\mathcal{H}_{\text{phy}}^{\text{wdw}}$ consists of positive frequency solutions $\underline{\Psi}(v, \phi)$ to (3.2) which are symmetric under the reversal of the orientation of the triad, i.e. satisfy $\underline{\Psi}(v, \phi) = \underline{\Psi}(-v, \phi)$, and which have a finite norm w.r.t. the inner product:

$$\langle \underline{\Psi}_1 | \underline{\Psi}_2 \rangle_{\text{phy}} = \int_{\phi=\phi_o} dv \underline{B}(v) \underline{\bar{\Psi}}_1(v, \phi) \underline{\Psi}_2(v, \phi) \quad (3.12)$$

where for notational simplicity here (and in what follows) we have dropped the subscript + denoting positive frequency. On this space, a useful complete set of Dirac observables is provided by the momentum \hat{p}_ϕ of the scalar field,

$$\hat{p}_\phi \underline{\Psi}(v, \phi) := -i\hbar \frac{\partial \underline{\Psi}(v, \phi)}{\partial \phi} \quad (3.13)$$

and the operator $|\hat{v}|_{\phi_o}$ corresponding to volume at the emergent time $\phi = \phi_o$,

$$|\hat{v}|_{\phi_o} \underline{\Psi}(v, \phi) = e^{i \sqrt{\Theta} (\phi - \phi_o)} |v| \underline{\Psi}(v, \phi_o). \quad (3.14)$$

Using the physical Hilbert space and this complete set of Dirac observables we can now introduce semi-classical states and study their evolution. Let us fix an ‘instant of time’ $\phi = \phi_o$ and construct a semi-classical state which is peaked at $p_\phi = p_\phi^*$ and $|v|_{\phi_o} = v^*$. Since we would like the peak to be at a point that represents a large classical universe, we are led to choose $v^* \gg 1$ and $p_\phi^* \gg \hbar$ (in the natural classical units $c=G=1$). The second condition is necessary to ensure that the universe expands out to a size much larger than the Planck scale. At ‘time’ $\phi = \phi_o$, consider the state

$$\underline{\Psi}(v, \phi_o) = \int_0^\infty dk \tilde{\Psi}(k) \underline{e}_k(v) e^{i\omega(\phi_o - \phi^*)}, \quad \text{where } \tilde{\Psi}(k) = e^{-\frac{(k-k^*)^2}{2\sigma^2}}. \quad (3.15)$$

Here

$$k^* = \sqrt{3/16\pi G \hbar^2} p_\phi^* \quad \text{and} \quad \phi^* = \phi_o + \sqrt{\frac{3}{16\pi G}} \cosh^{-1} \left[\left(\frac{3K^2(p_\phi^*)^2}{\ell_o^2 G \hbar^2 \gamma^2} \right)^{1/2} (v^*)^{-2/3} \right]. \quad (3.16)$$

In the spatially flat case, the eigenfunctions $e_k(v)$ were just plane waves [3] and one could evaluate this integral analytically. The modified Bessel functions are much more complicated. Therefore, in the closed model we have to use numerical methods. They show that

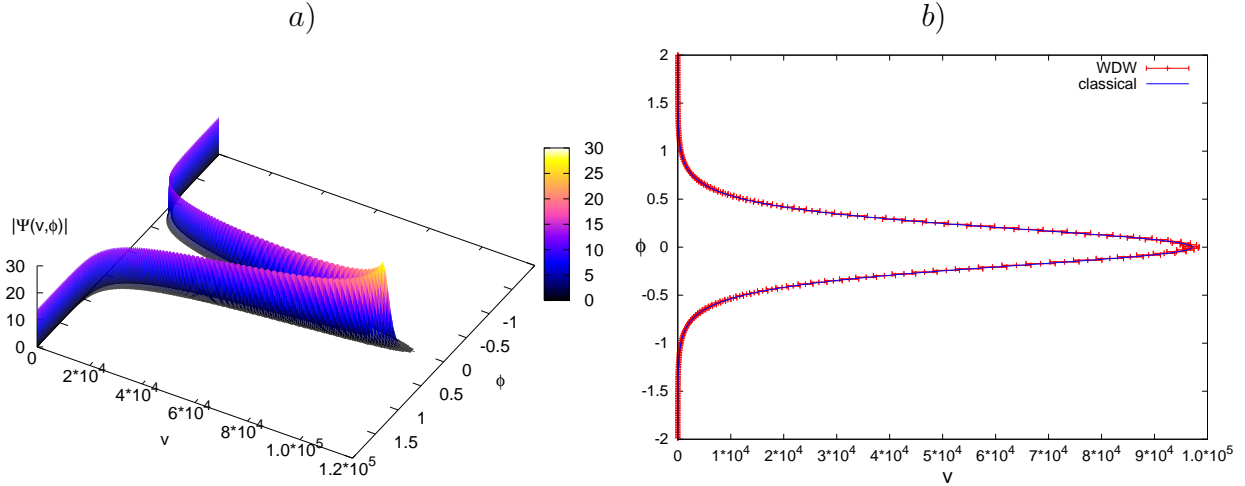


FIG. 1: *a)* The absolute value of the WDW wave function. The initial state at ‘time ϕ_o ’ was constructed using (3.15) and is sharply peaked at p_ϕ^* , and $v^*|_{\phi_o}$. It remains sharply peaked on the classical trajectory with $p_\phi = p_\phi^*$, passing through v^* at $\phi = \phi_o$. For clarity of visualization, only the values of $|\Psi|$ greater than 10^{-4} are shown. Being a physical state, Ψ is symmetric under $v \rightarrow -v$. In this simulation, the parameters were: $p_\phi^* = 5000$, and $\Delta p_\phi/p_\phi^* = 0.02$. *b)* The expectation values (and dispersions) of $|\hat{v}|_\phi$ are plotted for the WDW wave function and compared with the classical trajectory. The WDW wave function follows the classical trajectory into the big-bang and big-crunch singularities.

this state is sharply peaked at values v^* , p_ϕ^* of our Dirac observables (see Fig. 1a).

We can now ask for the evolution of this state. Does it remain peaked at the classical trajectory defined by $p_\phi = p_\phi^*$ and passing through $v = v^*$ at $\phi = \phi_o$? This question is easy to answer because (3.11) implies that the (positive frequency) solution $\underline{\Psi}(v, \phi)$ to (3.2) defined by the initial data (3.15) is obtained simply by replacing ϕ_o by ϕ in (3.15)! Since σ , the measure of dispersion in (3.15), does not depend on ϕ , it follows that $\underline{\Psi}(v, \phi)$ continues to be peaked at a trajectory which is precisely the classical solution of interest. This is just what one would hope during the epoch in which the universe is large. However, the property holds also in the Planck regime and the semi-classical state simply follows the classical trajectory into the big-bang and big crunch singularities. (See Figs. 1a and 1b.) In this sense, the WDW evolution does not resolve the classical singularity.

We will show in the next three sections that the situation is very different in LQC. This can occur because the WDW equation is a good approximation to the discrete equation only for large v . Furthermore, as discussed in [3], the approximation is not uniform but depends on the state: in arriving at the WDW equation from LQC we had to neglect Ψ dependent terms of the form $O(v^{n-3} \frac{d^n \Psi}{dv^n})$ for $n \geq 3$. For semi-classical states considered above, this implies that the approximation is excellent for $v \gg k^*$ but becomes inadequate when the peak of the wave function lies at a value of v comparable to k^* . Then, the LQC evolution departs sharply from the WDW evolution. We will find that, rather than following the classical trajectory into the big bang singularity, the peak of the LQC wave function now exhibits a bounce. Since large values of k^* are classically preferred, the value of v at the bounce can be quite large. However, as in the $k = 0$ models [3], we will find that the matter density at the bounce point is comparable to the Planck density, independently of

the precise value of k^* so long as $p_\phi^* \gg \hbar$.

IV. LOOP QUANTUM COSMOLOGY: ANALYTICAL ISSUES

Since generic solutions in the closed, $k=1$ cosmologies undergo a recollapse in classical general relativity, the scale factor can not serve as a global time variable. This fact has been used as a criticism of the implicit use of the scale factor as time in the older LQC literature (see, e.g., [6]). However, if matter sources *include* a massless scalar field ϕ , that field *is* monotonic and single valued in all classical solutions. Therefore it can be chosen as the ‘internal’ time variable with respect to which the scale factor and other fields evolve. Furthermore, as discussed in section II, for the model considered in this paper the Hamiltonian constraint (2.31) of LQC has the same form as the wave equation in a static space-time, with ϕ playing the role of time and Θ of the elliptic spatial operator plus a static potential. Therefore as in the $k=0$ case ϕ can be regarded as *emergent time* also in the quantum theory. This choice is free of the criticisms mentioned above.⁵ In this section we will construct the physical sector of LQC by exploiting this fact. As mentioned in section I, we will find that quantum geometry effects resolve both the big bang and the big crunch singularities, leading to a cyclic quantum universe. Still the scalar field will continue to be a viable emergent time *globally*.

A. General solution to the LQC Hamiltonian constraint

As in the spatially flat $k=0$ case, our kinematical Hilbert space will be: $\mathcal{H}_{\text{kin}}^{\text{total}} := L^2(\mathbb{R}_{\text{Bohr}}, B(v)d\mu_{\text{Bohr}}) \otimes L^2(\mathbb{R}, d\phi)$. Since ϕ is to be thought of as ‘time’ and v as the genuine, physical degree of freedom which evolves with respect to this ‘time’, we have chosen the standard Schrödinger representation for ϕ but the ‘polymer representation’ for v to correctly incorporate the quantum geometry effects. This is a conservative approach in that the results will directly reveal the manifestations of quantum geometry. Had we chosen a non-standard representation for the scalar field, these effects would have been mixed with those arising from an unusual representation of ‘time evolution’ and, furthermore, comparison with the WDW theory would have become more complicated.

The form of the LQC Hamiltonian constraint (2.31) is the same as that of the WDW constraint (3.2). Properties of Θ_o analyzed in [3] immediately imply that Θ is again a positive, symmetric operator on $L^2(\mathbb{R}_{\text{Bohr}}, B(v)d\mu_{\text{Bohr}})$, whence it admits a self-adjoint (Friedrich) extension. (For precise domains, see [10].) The main difference is that while the WDW $\underline{\Theta}$ is a differential operator, the LQC Θ is a *difference* operator. This gives rise to certain technically important distinctions. For, now the space of physical states —i.e. of appropriate solutions to the constraint equation— is naturally divided into sectors each of

⁵ Furthermore, as emphasized in [2, 3], while the availability of a global time variable simplifies the constructions considerably and makes physical interpretation transparent, it is not essential. Using the group averaging procedure [21], for example, the physical sector of the theory can be constructed even when a global intrinsic time does not exist. Furthermore, in simple examples [22] physical interpretation can be aided by the introduction of a suitable *local* notion of time which exists, e.g., if the scalar field comes with an inflationary potential.

which is preserved by the ‘evolution’ and by the action of our Dirac observables. Thus, there is super-selection. Let $\mathcal{L}_{|\varepsilon|}$ denote the ‘lattice’ of points $\{|\varepsilon| + 4n, n \in \mathbb{Z}\}$ on the v -axis, $\mathcal{L}_{-|\varepsilon|}$ the ‘lattice’ of points $\{-|\varepsilon| + 4n, n \in \mathbb{Z}\}$ and let $\mathcal{L}_\varepsilon = \mathcal{L}_{|\varepsilon|} \cup \mathcal{L}_{-|\varepsilon|}$ where as usual \mathbb{Z} denotes the set of integers. Let $\mathcal{H}_{|\varepsilon|}^{\text{grav}}$, $\mathcal{H}_{-|\varepsilon|}^{\text{grav}}$ and $\mathcal{H}_\varepsilon^{\text{grav}}$ denote the subspaces of $L^2(\mathbb{R}_{\text{Bohr}}, B(v)d\mu_{\text{Bohr}})$ with states whose support is restricted to lattices $\mathcal{L}_{|\varepsilon|}$, $\mathcal{L}_{-|\varepsilon|}$ and \mathcal{L}_ε . Each of these three subspaces is mapped to itself by Θ which is self-adjoint and positive definite on all three Hilbert spaces. However, for reasons explained in detail in [3], our physical states will be invariant under the orientation reversing operator Π of (3.1). Thus, we are primarily interested in the symmetric subspace of $\mathcal{H}_\varepsilon^{\text{grav}}$; the other two Hilbert spaces will be useful only in the intermediate stages of our discussion.

Our first task is to explore properties of the operator Θ . Since it is self-adjoint and positive definite, its spectrum is non-negative. Therefore as in the WDW theory we will denote its eigenvalues by ω^2 . On each Hilbert space $\mathcal{H}_{\pm|\varepsilon|}^{\text{grav}}$, we can solve for the eigenvalue equation $\Theta \psi_\omega(v) = \omega^2 \psi_\omega(v)$, i.e.,

$$\begin{aligned} & C^+(v) \psi_\omega(v+4) + C^o(v) \psi_\omega(v) + C^-(v) \psi_\omega(v-4) \\ & + \frac{\pi G}{2} \left[3K \left(\sin^2 \left(\frac{\bar{\mu} \ell_o}{2} \right) - \frac{\bar{\mu}^2 \ell_o^2}{4} \right) |v| - \frac{1}{3} \ell_o^2 \gamma^2 \left| \frac{v}{K} \right|^{\frac{1}{3}} \right] \left[||v-1| - |v+1|| \right] \psi_\omega(v) \\ & = \omega^2 B(v) \psi_\omega(v). \end{aligned} \quad (4.1)$$

Since this equation has the form of a second order recursion relation, as in the $k=0$ case one might expect a 2-fold degeneracy. However, there is an important subtlety. Let us consider the asymptotic regime $v \gg 1$. Then, each ψ_ω approaches a solution to the WDW equation and as we saw in section III A there is only one linearly independent solution which does not diverge for large v . The form of the inner product on $\mathcal{H}_\varepsilon^{\text{grav}}$ now implies that, as in the WDW theory, the degeneracy is removed; only one of the two linearly independent solutions can belong to the spectral family of Θ . Furthermore, numerical calculations show that this solution, which decays exponentially for $v \gg 1$, will in general diverge in the other asymptotic limit $-v \gg 1$. It is only for some *discrete* values ω_n of ω that one obtains solutions which do not diverge in either asymptotic limits. (This phenomenon was already noted in [9] in a simpler model without a scalar field but with a negative cosmological constant.) Since these solutions decay exponentially in both limits, they are normalizable in $\mathcal{H}_\varepsilon^{\text{grav}}$. Thus, in contrast to the $k=0$ case, on each superselected sector, the spectrum of Θ is *discrete and each of its eigenvalues is non-degenerate*.⁶ We will denote the normalized eigenfunctions in $\mathcal{H}_{|\varepsilon|}^{\text{grav}}$ by $e_n(v)$:

$$\Theta e_n(v) = \omega_n^2 e_n(v) \quad \text{and} \quad \langle e_m | e_n \rangle = \delta_{m,n}. \quad (4.2)$$

Finally, physical states will be built from eigenfunctions $e_n^{(s)}$ which are symmetric under orientation reversal. Since Θ commutes with the orientation reversal operator Π , $e_n(-v) =$

⁶ See [10] for an analytical proof which does not rely on numerical results. Recall that in the WDW theory the spectrum is non-degenerate but *continuous*. This difference arises because in the WDW theory the eigenfunctions oscillate more and more wildly as v goes to zero and thus fail to be normalizable in the WDW Hilbert space $L^2(\mathbb{R}, (K/v)dv)$. Because of the discreteness of lattices $\mathcal{L}_{\pm|\varepsilon|}$, nothing special happens ‘near’ $v = 0$ in LQC.

$\Pi e_n(v)$ is an eigenfunction of Θ with the same eigenvalue ω_n^2 as $e_n(v)$, but belongs to $\mathcal{H}_{-|\varepsilon|}^{\text{grav}}$ rather than $\mathcal{H}_{|\varepsilon|}^{\text{grav}}$. Therefore,

$$e_n^{(s)} = \frac{1}{\sqrt{2}} (e_n(v) + e_n(-v)), \quad (4.3)$$

also has eigenvalue ω_n^2 , but belongs to $\mathcal{H}_{\varepsilon}^{\text{grav}}$.

We can now write down the general symmetric solution to the quantum constraint (2.31) with initial data in $\mathcal{H}_{\varepsilon}^{\text{grav}}$:

$$\Psi(v, \phi) = \sum_n [\tilde{\Psi}_n^+ e_n^{(s)}(v) e^{i\omega_n \phi} + \tilde{\Psi}_n^- \bar{e}_n^{(s)}(v) e^{-i\omega_n \phi}] \quad (4.4)$$

where $\tilde{\Psi}_n^{\pm}$ are square-summable. As in the WDW theory, if $\tilde{\Psi}_n^-$ vanishes, we will say that the solution is of positive frequency and if $\tilde{\Psi}_n^+$ vanishes we will say it is of negative frequency. Thus, every solution to (2.31) admits a natural positive and negative frequency decomposition. The positive (respectively negative) frequency solutions satisfy a Schrödinger type first order differential equation in ϕ :

$$\mp i \frac{\partial \Psi_{\pm}}{\partial \phi} = \sqrt{\Theta} \Psi_{\pm} \quad (4.5)$$

with a Hamiltonian $\sqrt{\Theta}$ (which is non-local in v). Therefore the solutions with initial datum $\Psi(v, \phi_o) = f_{\pm}(v)$ are given by:

$$\Psi_{\pm}(v, \phi) = e^{\pm i \sqrt{\Theta} (\phi - \phi_o)} f_{\pm}(v, \phi). \quad (4.6)$$

To summarize, the overall structure is analogous to that in the spatially open, $k=0$ case. A key difference is that the spectrum of Θ is discrete on each of the three Hilbert spaces, $\mathcal{H}_{\pm|\varepsilon|}^{\text{grav}}$ and $\mathcal{H}_{\varepsilon}^{\text{grav}}$. In particular, while in the $k=0$ case all eigenfunctions have an oscillatory asymptotic behavior, now they all decay exponentially for sufficiently large $|v|$. This difference neatly encodes in the quantum theory the key qualitative difference between the two models in the classical theory: In the $k=0$ case any one classical solution is either ever expanding or ever contracting, while in the $k=1$ case each solution expands to a maximum volume and then recollapses.

B. The Physical sector

We will now summarize the mathematical structure of the physical sector of the theory. The construction is entirely analogous to that in the $k=0$ case since the spectrum of the full constraint operator $\partial_{\phi}^2 + \Theta$ is still continuous (because of the ∂_{ϕ}^2 part). Therefore we will only state the final results.

The sector of the physical Hilbert space $\mathcal{H}_{\text{phy}}^{\varepsilon}$ labeled by $\varepsilon \in [0, 2]$ consists of positive frequency solutions $\Psi(v, \phi)$ to (4.5) with initial data $\Psi(v, \phi_o)$ in the symmetric sector of

$\mathcal{H}_{\text{grav}}^\varepsilon$. Eq. (4.4) implies that they admit an explicit expansion

$$\Psi(v, \phi) = \sum_n \tilde{\Psi}_n e_n^{(s)}(v) e^{i\omega_n \phi}, \quad (4.7)$$

where, we have suppressed the superscript $+$ because from now on we will only work with positive frequency solutions. The physical inner product is given by

$$\langle \Psi_1 | \Psi_2 \rangle_\varepsilon = \sum_{v \in \{\pm|\varepsilon| + 4n; n \in \mathbb{Z}\}} B(v) \bar{\Psi}_1(v, \phi_o) \Psi_2(v, \phi_o) \quad (4.8)$$

for any ϕ_o . The action of the Dirac observables is independent of ε , and has the same form as in the WDW theory:

$$|\hat{v}|_{\phi_o} \Psi(v, \phi) = e^{i\sqrt{\Theta}(\phi - \phi_o)} |v| \Psi(v, \phi_o), \quad \text{and} \quad \hat{p}_\phi \Psi(v, \phi) = -i\hbar \frac{\partial \Psi(v, \phi)}{\partial \phi}. \quad (4.9)$$

The kinematical Hilbert space $\mathcal{H}_{\text{kin}}^{\text{total}}$ is non-separable but, because of super-selection, each physical sector $\mathcal{H}_{\text{phy}}^\varepsilon$ is separable. Eigenvalues of the Dirac observable $|\hat{v}|_{\phi_o}$ constitute a discrete subset of the real line in each sector. The set of these eigenvalues in different sectors is distinct. Therefore which sector actually occurs is a question that can be in principle answered experimentally, provided one has access to microscopic measurements which can distinguish between values of the scale factor which differ by about a Planck length. This will not be feasible in the foreseeable future. Of greater practical interest are the coarse-grained measurements, where the coarse graining occurs at significantly greater scales. For these measurements, different sectors would be indistinguishable and one could work with any one.

V. LOOP QUANTUM COSMOLOGY: NUMERICAL ISSUES

As we saw in section IV physical states can be readily constructed from eigenfunctions of the difference operator Θ . In the first part of this section, we study properties of these eigenfunctions. We show that Θ *admits only normalizable eigenfunctions with discrete eigenvalues* and numerically construct an orthonormal basis. In the second part we use this basis to construct and analyze physical semi-classical states.

A. Spectrum of Θ

Eigenfunctions of Θ are solutions to the difference equation (4.1). Since its coefficients are real, any eigenfunction can be expressed as a complex linear combination of real eigenfunctions. Therefore, it will suffice to restrict ourselves to real eigenfunctions.

Consider a generic lattice \mathcal{L}_ε , i.e., a lattice where ε does not equal 0 or 2. Since $\mathcal{L}_\varepsilon = \mathcal{L}_{|\varepsilon|} \cup \mathcal{L}_{-|\varepsilon|}$, to obtain an eigenfunction which is symmetric under orientation reversal $v \rightarrow -v$ it suffices to solve the eigenvalue equation just on $\mathcal{L}_{|\varepsilon|}$ and then reflect it. Because Θ is invariant under orientation reversal, the reflected function is automatically an eigenfunction with the same eigenvalue, but supported on $\mathcal{L}_{-|\varepsilon|}$. Furthermore, if the original eigenfunction is normalizable on $\mathcal{L}_{|\varepsilon|}$, the reflected one is normalizable on $\mathcal{L}_{-|\varepsilon|}$ whence the sum is a

symmetric, normalizable eigenfunction on \mathcal{L}_ε . Therefore, in what follows, *for a generic ε we will restrict ourselves to $\mathcal{L}_{|\varepsilon|}$ and examine all eigenfunctions*. Since lattices with $\varepsilon = 0$ or 2 are symmetric under reflection, *on these exceptional lattices we will restrict ourselves only to symmetric eigenfunctions*.

Every such eigenfunction $\psi_\omega(v)$ is uniquely determined by its ‘initial’ values $\psi_\omega(\varepsilon + 4n)$, $\psi_\omega(\varepsilon + 4(n + 1))$ for some integer n .⁷ For later convenience, we note that the initial data can be represented by a pair of real parameters $b \in \mathbb{R}$ and $\theta \in [0, \pi]$

$$\psi_\omega(\varepsilon + 4n) = b \cos(\theta), \quad \psi_\omega(\varepsilon + 4(n + 1)) = b \sin(\theta). \quad (5.1)$$

Thus on generic lattices, for any ω , the eigenspace is *2-dimensional* and the degeneracy is parameterized by b, θ . On the exceptional lattices, the symmetry requirement imposes an additional constraint which determines $\psi_\omega(\varepsilon + 4)$ as function of $\psi_\omega(\varepsilon)$. Therefore on these lattices the eigenspace is only *one dimensional*.

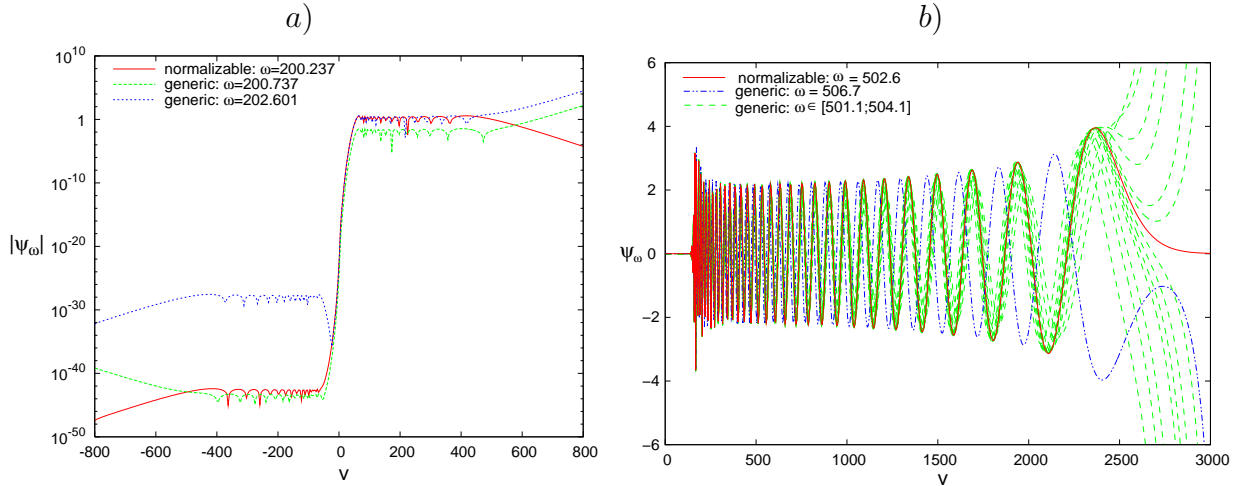


FIG. 2: Examples of normalizable and generic eigenfunctions of Θ . The plot *a)* presents eigenfunctions supported on the lattice with $\varepsilon = 0.5$. Since the scale on the y-axis is logarithmic, it is clear that in the asymptotic region generic eigenfunctions diverge exponentially while the normalizable ones decay exponentially. Plot *b)* shows eigenfunctions supported on the $\varepsilon = 0$ lattice. Since the scale on the y-axis is linear this plot brings out the detailed behavior of eigenfunctions in the region where $|\psi_\omega|$ is small.

The generic behavior of eigenfunctions $\psi_\omega(v)$ is shown in Fig 2. One can distinguish three regions on the positive (or negative) v axis in each of which the eigenfunction $\psi_\omega(v)$ has a qualitatively different behavior.

- (i) Genuine quantum region: $|v| \lesssim v_b$ in which $|\psi_\omega|$ grows/decays exponentially. For $\varepsilon = 0$ or 2, $|\psi_\omega|$ always grows with $|v|$. v_b turns out to be proportional to ω .

⁷ If $\varepsilon \neq 2$, the eigenvalue equation (4.1) recursively determines $\psi_\omega(v)$ on the entire $\mathcal{L}_{+|\varepsilon|}$. If $\varepsilon = 2$ the coefficients $C^-(2)$ and $C^+(-2)$ in Eq. (4.1) vanish. Therefore, we can calculate $\psi_\omega(v)$ only on half of the v axis. However, values of $\psi_\omega(v)$ on the other half are determined by the symmetry condition.

- (ii) ‘Semi-classical’ region: $v_b \lesssim |v| \lesssim v_r$ in which ψ_ω oscillates. v_r turns out to be proportional to $\omega^{3/2}$ (and approximately equals the maximal $|v|$ of a classical universe of momentum $p_\phi = \hbar\omega$).
- (iii) Classically forbidden region: $|v| \gtrsim v_r$, where ψ_ω grows/decays exponentially as $|v|$ increases.

(However, numerical simulations show that the distinction between first two regions gets blurred for eigenfunctions corresponding to $\omega \lesssim 5$.) Note that for a generic lattice, the eigenfunction may decay in one asymptotic region (say, $v \rightarrow \infty$) but grow in the other ($v \rightarrow -\infty$). Eigenfunctions growing on either side fail to be normalizable, whereas the ones decaying for both signs of v are normalizable. While eigenfunctions exist for any ω , they decay on both sides only for certain discrete values of ω . Consequently the spectrum of Θ is discrete and the normalizable eigenfunctions form a set of zero measure in the space of all eigenfunctions. We will now describe the search algorithm to find them. We begin with the simpler case of $\varepsilon = 0$ or 2 lattices and then discuss the more subtle case of generic lattices.

Fix $\varepsilon = 0$ or 2. Because of symmetry, it suffices to analyze the behavior of $\psi_\omega(v)$ just for $v > 0$. Let us focus on an interval $W = [\omega_1, \omega_2]$ of frequencies and fix a point $v' \in \mathcal{L}_\varepsilon$ such that $v' \gg v_r(\omega_2)$. Eq. (4.1) implies that the value $\psi_\omega(v')$ is a continuous function of $\psi_\omega(v)|_{v=\varepsilon}$ and ω . One can fix the initial value $\psi_\omega(\varepsilon)$ to 1, thus leaving the dependence only on ω . Numerical inspection shows that $\psi_\omega(v)$ changes sign quasi-periodically as ω increases (see the right plot of Fig. 2). Let us take one of the (possibly many) values $\omega_{n,v'}$ such that $\psi_{\omega_{n,v'}}(v)|_{v=v'} = 0$. The limits

$$\omega_n = \lim_{v' \rightarrow \infty} \omega_{n,v'} \quad (5.2)$$

are the only eigenvalues corresponding to normalizable eigenfunctions. In practice the values $\omega_{n,v'}$ for $v' \approx 1.3v_r$ approximate the limiting value ω_n with precision 10^{-16} .

In actual calculations the following algorithm was applied:

- (i) First we consider a set of frequency values ω_i uniformly distributed within the interval $[0, \omega_{\max}]$. For each fixed v' , the separation $\omega_{i+1} - \omega_i$ was chosen to be much smaller than separation between values of ω at which $\psi_\omega(v')$ vanishes. (In practice the separations turned out to be greater than 1 for $\omega < 3 \times 10^5$.)
- (ii) Whenever the change of sign between $\psi_{\omega_{i+1}}(v')$ and $\psi_{\omega_i}(v')$ was detected, the value $\omega_{n,v'}$ corresponding to the root of $\psi_\omega(v')$ was found via bisection method.

For this scan, ω_{\max} was chosen as 3×10^5 . The first of the two steps in the algorithm ensures that all eigenfunctions in the chosen interval have been found.

Let us now consider a generic lattice. Now there are two factors which complicate the task of finding normalizable eigenfunctions. First, the eigenspaces are *two* dimensional, parameterized by b, θ as in (5.1). Therefore, even if we fix the normalization freedom by setting $b = 1$, for each frequency ω we have a *1-parameter family* of eigenfunctions, labeled by θ (rather than a single eigenfunction as on $\varepsilon = 0$ or 2 cases). Secondly, since the desired eigenfunctions do not have to be symmetric on $\mathcal{L}_{|\varepsilon|}$, now we have to analyze the behavior of ψ_ω when $|v| \gg v_r$ *separately for positive and negative values* of v . We therefore modified the algorithm specified for the $\varepsilon = 0$ or 2 lattices as follows.

First, keeping ω fixed and varying θ instead of ω in the above procedure, we searched for $\psi_\omega(v)$ which decays on the *negative v side*. For this we probed the domain of θ in 100

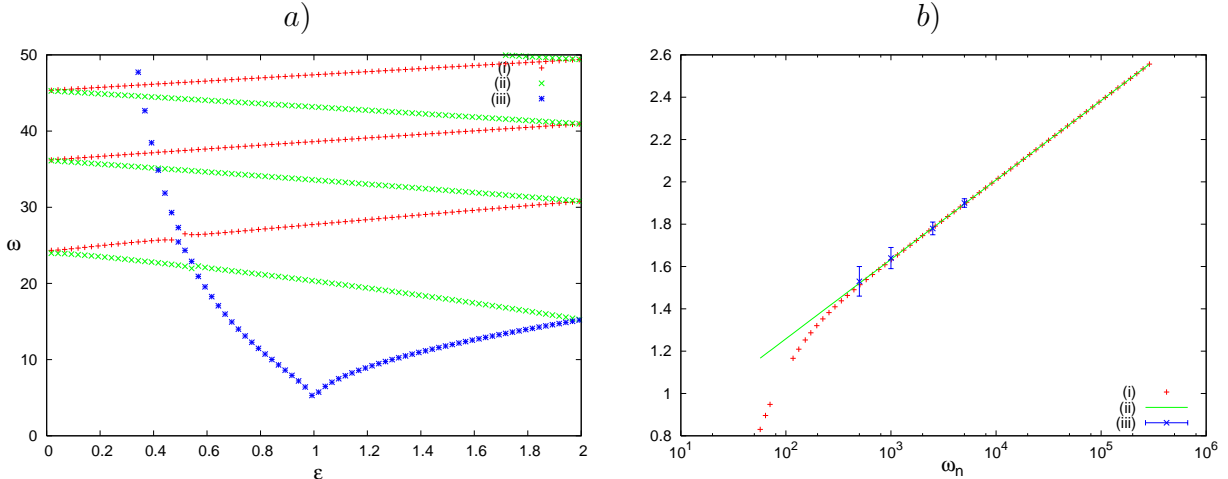


FIG. 3: *a)* Distribution of lowest ($\omega < 50$) eigenvalues (corresponding to normalizable eigenfunctions) for different ε . Eigenvalues are divided into three classes according to the behavior of eigenfunctions, which are i) suppressed for $v < 0$, ii) suppressed for $v > 0$, and iii) large only near $v = 0$. *b)* Rescaled spectral density $2\pi/(\omega_n - \omega_{n-1})$ (i) is compared with periods $T_\phi(\omega_n)$ in ϕ (iii) of expectation value of $|\hat{v}|_\phi$ of the coherent states evolved from the WDW initial data (see section VB). The solid line (ii) shows the large ω limit of the rescaled spectral density.

points uniformly distributed within $[0, \pi]$ and, whenever sign of $\psi_\omega(v')$ changed, we narrowed the choices of θ using bisection. The analysis shows that for each ω there exists *unique* θ such that ψ_ω satisfies this condition. With θ so determined, we again have a 1-dimensional eigenspace $\psi_\omega(v)$ for each ω . Therefore, we could now apply the procedure used for $\varepsilon = 0$ or 2 to look for eigenfunctions which decay *on the positive side*. Thus the two complications so to say compensate one another: while there is an additional, 1-dimensional freedom (labeled by θ) in the choice of eigenfunctions, since the requirement that the eigenfunctions decay on the negative v side is now decoupled from the requirement that they decay on the positive side, we have an additional constraint (which determines θ for any given ω). Therefore, the only modification to the algorithm used in the $\varepsilon = 0$ or 2 cases was to first determine θ .

To gain insight into the qualitative features of eigenfunctions and eigenvalues, this method was first applied to $\omega \in [0, 50]$ by choosing $\mathcal{L}_{+|\varepsilon|}$. Normalized eigenfunctions decay exponentially as $|v|$ increases for both positive and negative v . It was found that these eigenfunctions generically have an additional feature: in the ‘semi-classical’ region described above, their values on the positive or negative sides of the v axis are suppressed relative to their values on the other half, the difference in the amplitudes growing exponentially with ω . Since we will be primarily interested in large ω , if the initial data are specified on the side where ψ_ω is large, the suppression on the other side enhances the numerical errors making the results unreliable. For these cases, the search of normalizable eigenfunctions was performed again, now starting from the side where ψ_ω is small.

After implementing all these precautions to control errors, a much more exhaustive search for eigenvalues and eigenfunctions was made. The results can be summarized as follows.

- (i) The spectrum of Θ is discrete for all lattices. Each of its eigenvalues is non-degenerate. Normalizable eigenfunctions decay exponentially as $|v|$ tends to infinity.

- (ii) For generic ε , the restrictions to sublattices $\mathcal{L}_{\pm|\varepsilon|}$ of eigenfunctions $\psi_n(v)$ are in general strongly suppressed for one sign of v . The side on which suppression occurs depends on parity of n .
- (iii) The density of eigenvalues has following features. As shown in Fig. 3a it is roughly independent of ε except that for generic lattices it is twice as large as that for exceptional ones. It slowly grows with ω (see Fig. 3b). The best fit to the data in Fig. 3b leads to the behavior in large ω limit as:

$$\omega_n - \omega_{n-1} \rightarrow \frac{1}{\alpha \ln |\omega_n/\beta|} \quad (5.3)$$

with $\alpha = [0.0259272 \pm (5 \times 10^{-7})]G^{-1/2}$ and $\beta = [0.04412 \pm (1 \times 10^{-5})]G^{1/2}$.

- (iv) A state $\Psi(v)$ which is sharply peaked at some ω^* can be well-approximated by a linear combination only of eigenfunctions with eigenvalues lying in a small compact interval around ω^* . If ω^* is very large the estimate given in (iii) above implies that the distribution of ω_n is approximately uniform. Consequently, the wave function will be approximately periodic in ϕ with a period

$$T_\phi(\omega_n) \approx \frac{2\pi}{\omega_n - \omega_{n-1}}. \quad (5.4)$$

For an LQC physical state obtained from evolution of the initial data at $\phi = \phi_o$ corresponding to a WDW coherent state (see section VB), the period of expectation value $\langle |\hat{v}|_\phi \rangle$ turns out to be in good agreement with T_ϕ . This provides an independent check on our numerical analysis.

B. Evaluation of Semi-classical State and Observables

The numerical method presented in previous subsection allow us to find all the eigenstates of Θ which span the physical Hilbert space. To obtain the normalized eigenbasis $e_n^{(s)}$ (which is symmetric under orientation reversal) we first note that in the expression of the norm it suffices to evaluate just a finite sum

$$\|\psi_n\|_\varepsilon^2 = \sum_{v \in \{\pm\varepsilon+n; -N < n < N\}} B(v)\psi_n^2(v), \quad \text{where } N > \frac{v_r}{4}. \quad (5.5)$$

since $\psi_n(v)$ decay exponentially for $|v| > v_r \propto \omega^{\frac{3}{2}}$. With the basis at hand, one can construct physical states which are semiclassical at late times. As in $k = 0$ case [2], this can be done in two different ways:

- (i) Direct evaluation of the wave function using (4.7), and
- (ii) Evolution in ϕ of the initial data specified at $\phi = \phi_o$ using Eq. (2.31). (The initial data can be chosen to be the same as that of a semi-classical solution to the WDW equation at some late ‘time’ (see section III)).

The direct evaluation of the integral expression (4.7) already provides the full LQC solution. However, we also used this expression to obtain just the initial data at $\phi = \phi_o$ and

then evolved this data using (2.31). Agreement between the two solutions provides an independent check on numerics. Finally, we also evolved the initial data extracted from a WDW coherent state and used the resulting LQC solution thereby obtaining an independent check on completeness of the eigenbasis constructed in section V A. The rest of this section provides the relevant details of the numerical implementation of this procedure.

In order to evaluate the integral solution, we need the spectral profile $\tilde{\Psi}_n$ used in the expansion (4.4). Since we are primarily interested in states which are semiclassical at late times representing a macroscopic universe, we chose a Gaussian profile peaked around large ω^* : $\tilde{\Psi}_n = \exp(-(\omega_n - \omega^*)^2/(2\sigma^2))$. Since the contribution from eigenfunctions corresponding to ω sufficiently far away from ω^* can be neglected, to calculate $\Psi(v, \phi)$ via (4.7) one has to only sum a finite number of terms. In numerical simulations the summation in (4.7) was restricted to n such that $\omega^* - 10\sigma < \omega_n < \omega^* + 10\sigma$.

To calculate the initial data from the WDW coherent state we evaluated (3.15). Now the eigenfunctions $e_k(v)$ are appropriately normalized Bessel functions \mathcal{K}_{ik} . They were calculated using methods of Gil, Segura and Temme [24]. As in the initial data construction discussed in the last para, it is sufficient to restrict the domain of integration to a compact set $[k^* - 10\sigma; k^* + 10\sigma]$. Resulting integral was then numerically evaluated using a simple trapezoid method with set of 10^4 ‘probing’ points distributed uniformly. On the one hand, this calculation immediately leads to the solution to the WDW equation presented in Fig. 1. On the other, it provides us LQC initial data for any lattice \mathcal{L}_ε which was evolved using (2.31).

Eq. (2.31) constitutes a countable number of ordinary differential equations. Its domain in v is the lattice \mathcal{L}_ε . However, as noted in section V A, the symmetry of the wave function allows us to restrict the calculations to the sublattice $\mathcal{L}_{+|\varepsilon|}$ for generic ε and to the part $v > 0$ in the exceptional cases $\varepsilon = 0$ or 2 . Due to technical limitations the size of the domain was restricted by requiring that its elements v_i satisfy the inequality $|v_i - \varepsilon| \leq 4N \gg v_r(\omega^*)$. To ensure that the system remains closed, we impose boundary conditions on the outermost points $|v_i - \varepsilon| = 4N$ in the generic case and at the right outermost point $v_i - \varepsilon = 4N$ in the exceptional cases. Since these points lie deep in the classically forbidden region for all the eigenvalues contributing significantly to the state, one can safely impose reflective boundary conditions

$$\Psi(\pm 4N + \varepsilon, \phi) = \partial_\phi \Psi(\pm 4N + \varepsilon, \phi) = 0. \quad (5.6)$$

In actual simulations we chose $4N \approx 1.3v_r(\omega^*)$ which was sufficient for the boundary condition to not affect the dynamics.

The resulting finite set of equations was integrated using adaptive 4th order Runge-Kutta method. To estimate the numerical errors due to discretization in ϕ , restrictions $\Psi|_\phi$ calculated for different step sizes were compared using sup-norm

$$\|f\|(\phi) = \sup_{|v_i - \varepsilon| \leq 4N} f(v_i, \phi). \quad (5.7)$$

The step sizes $\Delta\phi$ were chosen to satisfy the inequality

$$\|\Psi_{\Delta\phi} - \Psi_{\Delta\phi/2}\| \leq \epsilon \|\Psi_{\Delta\phi/2}\| \Delta\phi \quad (5.8)$$

for small preset ϵ , where $\Psi_{\Delta\phi}$ and $\Psi_{\Delta\phi/2}$ are profiles calculated with step sizes $\Delta\phi$ and $\Delta\phi/2$ respectively. The dependence of $\|\Psi_{\Delta\phi} - \Psi_{\Delta\phi/2}\|$ on the number of steps of the integration for one of the calculations is presented in Fig. 4. It shows that the numerical errors mani-

fest themselves mainly in phases. The differences between the absolute values of the wave function profiles are approximately one order of magnitude smaller. Thus the expectation values and dispersions of observables $|\hat{v}|_\phi$ are determined with much better precision than Ψ itself.

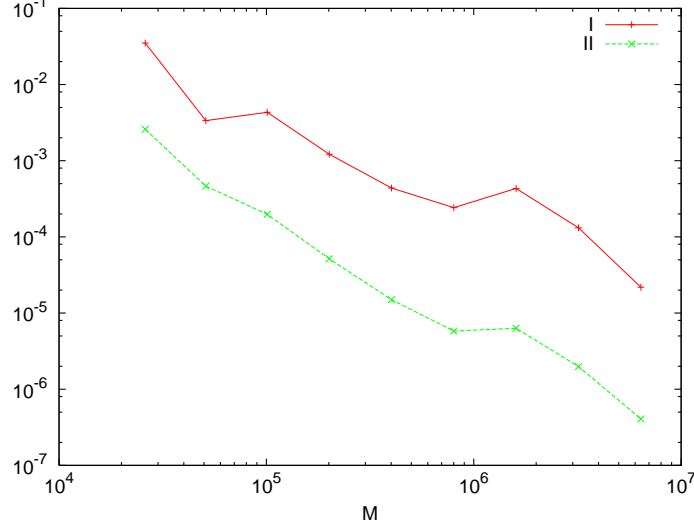


FIG. 4: Error functions $\|\Psi_{(M)} - \Psi\|/\|\Psi\|$ (upper curve) and $||\Psi_{(M)}| - |\Psi|||/\|\Psi\|$ (lower curve) are plotted as a function of the number of time steps. Here $\Psi_{(M)}$ refers to final profile of wave function for a simulation with M time steps. Ψ is the limit of final profile as $1/M \rightarrow 0$ calculated via polynomial extrapolation. In both cases, the evolution began at $\phi = 0$ and the final profile is evaluated at $\phi = -1$. Values of parameters are $p_\phi^* = 1000$, $\Delta p_\phi/p_\phi = 0.018$, $v^* = 4000$ and $\varepsilon = 0$.

The resulting wave functions $\Psi(v, \phi)$ were finally used to calculate the expectation values $\langle \hat{p}_\phi \rangle$, $\langle |\hat{v}|_\phi \rangle$ of observables defined by (4.9). With the inner product $\langle \Psi | \Psi \rangle_\varepsilon$ given by (4.8) they are equal to the following sums over $\mathcal{L}_{\varepsilon, N} := \{v = \pm\varepsilon + 4n; -N \leq n \leq N\}$

$$\langle \Psi | |\hat{v}|_\phi | \Psi \rangle = \langle \Psi | \Psi \rangle_\varepsilon^{-1} \sum_{v \in \mathcal{L}_{\varepsilon, N}} B(v) |v| |\Psi(v, \phi)|^2 \quad (5.9a)$$

$$\langle \Psi | \hat{p}_\phi | \Psi \rangle = \langle \Psi | \Psi \rangle_\varepsilon^{-1} \sum_{v \in \mathcal{L}_{\varepsilon, N}} B(v) \bar{\Psi}(v, \phi) (-i\hbar) \partial_\phi \Psi(v, \phi) \quad (5.9b)$$

The dispersions corresponding to considered observables were calculated via

$$\langle \Delta \hat{p}_\phi \rangle^2 = \langle \hat{p}_\phi^2 \rangle - \langle \hat{p}_\phi \rangle^2 \quad (5.10a)$$

$$\langle \Delta |\hat{v}|_\phi \rangle^2 = \langle \hat{v}_\phi^2 \rangle - \langle |\hat{v}|_\phi \rangle^2 \quad (5.10b)$$

where the expectation values $\langle \hat{p}_\phi^2 \rangle$ and $\langle \hat{v}_\phi^2 \rangle$ are of the form (5.9).

In actual simulations ω^* ranged from 500 to 10^4 , with relative uncertainties $\Delta\omega/\omega$ between 7×10^{-3} and 2.5×10^{-2} . Wave functions were calculated on lattices \mathcal{L}_ε corresponding to 5 different values of ε . Peaks in v of initial profiles were chosen to be no smaller than half of the maximal v predicted by classical theory. For example for $p_\phi^* = 500$, $v^* \approx 2000$ whereas

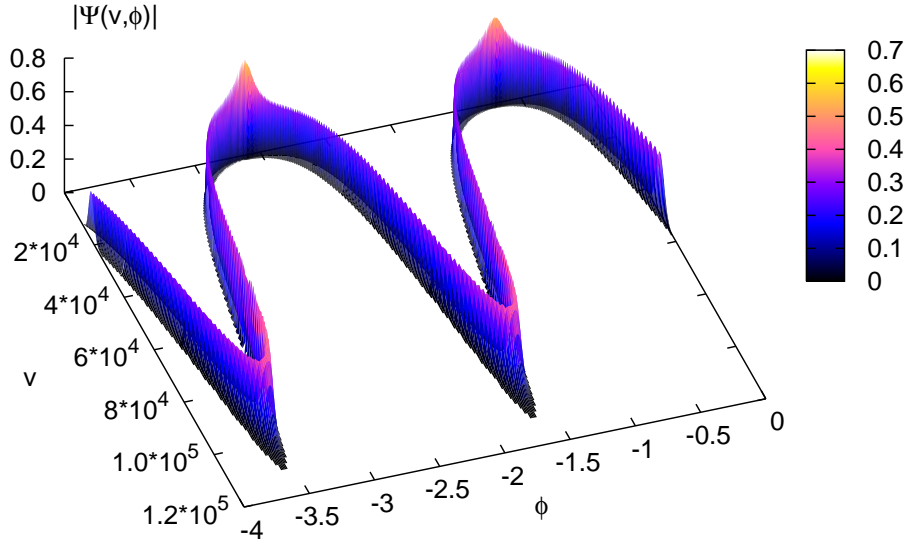


FIG. 5: The absolute value of the wavefunction obtained by numerical evolution. For visual clarity, only values $|\Psi| > 10^{-4}$ are shown. Parameters of the initial data are: $p_\phi^* = 5 \times 10^3$, $\Delta p_\phi/p_\phi = 0.018$, $v^* = 5 \times 10^4$ and $\varepsilon = 0$. Because of bounces the quantum universe exhibits a ‘cyclic’ character.

for $p_\phi^* = 5000$ the value of v^* ranged between $5 - 6 \times 10^4$. Evolution was performed in both forward and backward direction. Representative results of numerical evaluation of $|\Psi(v, \phi)|$ and the expectation values of $|\hat{v}|_\phi$ are shown in Figs. 5 and 6. Detailed discussion of the properties of $|\Psi(v, \phi)|$, the comparison of classical and quantum evolution and a summary of our results is presented in Sec. VIB.

VI. PHYSICAL IMPLICATIONS

In this section we discuss the physics of our numerical simulations. We first obtain the quantum corrected effective Friedmann equation and show that it is an excellent approximation to the numerical quantum evolution. We then list the numerical results and compare and contrast the exact quantum evolution, the effective theory and the classical Friedmann dynamics.

A. Effective Equations

The right hand side of the standard Friedmann equation

$$H^2 \equiv \left(\frac{\dot{a}}{a}\right)^2 \equiv \left(\frac{\dot{v}}{3v}\right)^2 = \frac{8\pi G}{3} \rho - \frac{1}{a^2} \quad (6.1)$$

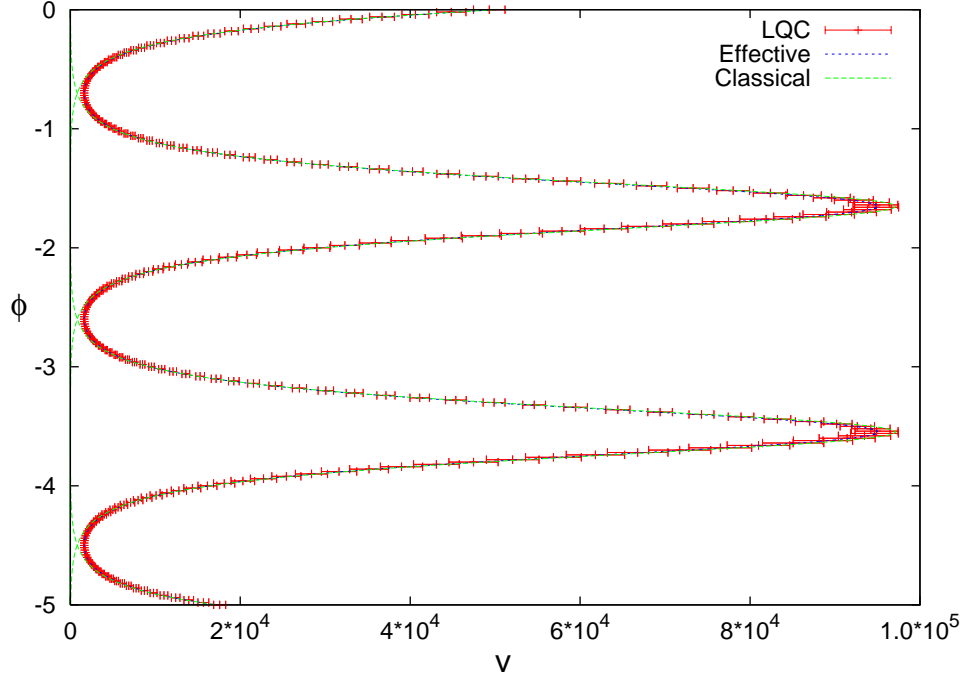


FIG. 6: Expectation values and dispersion of $|\hat{v}|_\phi$ for the wavefunction in Fig. 5 are compared with the classical trajectory and the trajectory from effective Friedmann dynamics obtained from Eqs.(6.3) and (6.4). The classical trajectory deviates significantly from the quantum evolution at Planck scale and evolves into singularities. The effective trajectory provides an excellent approximation to quantum evolution at all scales.

vanishes if and only if $\rho = 3/8\pi G a^2$. In any classical solution, at this point the scale factor reaches its maximum value, the matter density its minimum value, and the classical dynamics exhibits a turning point from an expanding phase to a contracting phase. Our numerical simulations show that quantum dynamics retains this turning point but also gives rise to additional turning points, resolving the big bang and the big crunch singularities (see Fig. 5). To gain an analytical understanding of the physics underlying this phenomenon, in this subsection we will obtain the leading LQC corrections to the classical Friedmann equation. This quantum corrected or ‘effective’ Friedmann equation already suffices to describe the behavior of the peak of wave functions that we found numerically in section V (see Fig. 6).

The procedure for obtaining these effective equations is the same as that in the $k=0$ case. Let us begin with a brief summary of the main ideas. One begins with a geometrical formulation of quantum mechanics in which the space of pure quantum states is represented an infinite dimensional symplectic manifold Γ_{quan} —called the *quantum phase space* (see, e.g., [25]). The quantum phase space has the structure of a fiber bundle: the base space is the classical phase space Γ_{class} and the infinite dimensional fiber over any point (q_o, p_o) of Γ_{class} is the space of quantum states in which the expectation values of the canonically conjugate operators (\hat{q}, \hat{p}) are (q_o, p_o) .⁸ Interestingly, the exact quantum dynamics provides a Hamiltonian flow on the symplectic manifold Γ_{quan} (the corresponding Hamiltonian being

⁸ In LQC (and LQG) an important subtlety arises because there is no operator corresponding to the

just the expectation value function of the quantum Hamiltonian operator). To obtain the desired, first order quantum corrections, one finds a cross-section of Γ_{quan} —i.e., an embedding of Γ_{class} into Γ_{quan} — to which this flow is approximately tangential in a well-defined sense [26]. This approximate quantum Hamiltonian flow unambiguously projects down to Γ_{class} and provides the desired corrections to classical equations of motion. In a certain sense this procedure encapsulates the more familiar ‘effective action’ calculations in the Hamiltonian framework [27]. In LQC, these quantum corrections have been obtained for various matter sources [26, 28], where judiciously chosen generalized coherent states are used to define the required embedding of Γ_{class} into Γ_{quan} . Just as the standard effective action refers to the in and out vacuum states, the final effective Hamiltonian (and thus the Friedmann and Raychaudhuri equations) depend on the specific choice of coherent states. However, the first order corrections we are interested in are insensitive to these details. In our case, the resulting effective Hamiltonian is:

$$\mathcal{H}_{\text{eff}} := \frac{C_{\text{eff}}}{16\pi G} = \frac{A(v)}{16\pi G} \left[\sin^2 \bar{\mu} \left(c - \frac{\ell_o}{2} \right) - \sin^2 \left(\frac{\bar{\mu} \ell_o}{2} \right) + (1 + \gamma^2) \frac{\bar{\mu}^2 \ell_o^2}{4} \right] + \left(\frac{8\pi\gamma\ell_{\text{Pl}}^2}{6} \right)^{-\frac{3}{2}} B(v) \frac{p_\phi^2}{2}. \quad (6.2)$$

where $A(v)$ denotes eigenvalues (2.26) of \hat{A} .

Since the Friedmann equations involve \dot{a}/a , to obtain modifications, we first derive the Hamilton’s equations of motion:

$$\begin{aligned} \dot{v} &= \{v, \mathcal{H}_{\text{eff}}\} = -\frac{8\pi\gamma G}{3} \frac{\partial \mathcal{H}_{\text{eff}}}{\partial c} \frac{\partial v}{\partial p} \\ &= -\frac{\gamma \bar{\mu} A(v)}{2} \left(\frac{8\pi\gamma\ell_{\text{Pl}}^2}{6} \right)^{-1} K^{2/3} |v|^{1/3} \sin \bar{\mu} \left(c - \frac{\ell_o}{2} \right) \cos \bar{\mu} \left(c - \frac{\ell_o}{2} \right) \end{aligned} \quad (6.3)$$

and

$$\dot{\phi} = \{\phi, \mathcal{H}_{\text{eff}}\} = \left(\frac{8\pi\gamma\ell_{\text{Pl}}^2}{6} \right)^{-3/2} B(v) p_\phi. \quad (6.4)$$

Using the constraint equation $\mathcal{H}_{\text{eff}} = 0$, i.e.,

$$\sin^2 \bar{\mu} \left(c - \frac{\ell_o}{2} \right) = \left(\sin^2 \left(\frac{\bar{\mu} \ell_o}{2} \right) - (1 + \gamma^2) \frac{\bar{\mu}^2 \ell_o^2}{4} \right) - 8\pi G \left(\frac{8\pi\gamma\ell_{\text{Pl}}^2}{6} \right)^{-\frac{3}{2}} B(v) \frac{p_\phi^2}{A(v)}, \quad (6.5)$$

we can eliminate the dependence on the connection c in (6.3) and obtain the desired quantum-corrected Friedmann equation

$$\begin{aligned} H^2 &= \frac{\gamma^2 \bar{\mu}^2 A(v)^2}{(8\pi\gamma\ell_{\text{Pl}}^2)^2} \left(\frac{K}{|v|} \right)^{4/3} \left[\sin^2 \left(\frac{\bar{\mu} \ell_o}{2} \right) - (1 + \gamma^2) \frac{\bar{\mu}^2 \ell_o^2}{4} - 8\pi G \left(\frac{8\pi\gamma\ell_{\text{Pl}}^2}{6} \right)^{-\frac{3}{2}} B(v) \frac{p_\phi^2}{A(v)} \right] \\ &\quad \times \left[1 - \sin^2 \left(\frac{\bar{\mu} \ell_o}{2} \right) - (1 + \gamma^2) \frac{\bar{\mu}^2 \ell_o^2}{4} + 8\pi G \left(\frac{8\pi\gamma\ell_{\text{Pl}}^2}{6} \right)^{-\frac{3}{2}} B(v) \frac{p_\phi^2}{A(v)} \right], \end{aligned} \quad (6.6)$$

which, as with the classical Friedmann equation (6.1), involves only v , \dot{v} and p_ϕ . To take the

configuration variables, i.e., the connections. One has to use holonomies instead. This issue is handled in [26].

classical limit, we note that the volume is given by $(8\pi\gamma/6)^{3/2}(|v|/K)\ell_{\text{Pl}}^3$ and that (the area gap and hence) $\bar{\mu}$ goes to zero in this limit. Therefore, in the limit (6.6) reduces precisely to (6.1). Terms containing $\bar{\mu}$ represent the quantum geometry corrections.

In view of the fact that the quantum equations are invariant under the orientation reversal map $\Pi \Psi(v) = \Psi(-v)$, it will suffice to restrict ourselves to $v \geq 0$. Now, for $v > 1$ we have

$$A(v) = -\frac{\sqrt{48\pi}}{\gamma^{3/2}\bar{\mu}^2} \left(\frac{|v|}{K}\right)^{1/3} \ell_{\text{Pl}} \quad (6.7)$$

and for $v \gg 1$, we have:

$$B(v) = \frac{K}{v} + O(v^{-3}) \quad (6.8)$$

Therefore, the leading order quantum corrected equation is given by:

$$\begin{aligned} H^2 = & \left(\frac{8\pi G}{3} \rho + \frac{1}{\gamma^2 \bar{\mu}^2} \left(\frac{8\pi\gamma\ell_{\text{Pl}}^2}{6} \right)^{-1} \left(\frac{K}{|v|} \right)^{2/3} \left(\sin^2 \left(\frac{\bar{\mu}\ell_o}{2} \right) - (1 + \gamma^2) \frac{\bar{\mu}^2 \ell_o^2}{4} \right) \right) \\ & \times \left(1 - \sin^2 \left(\frac{\bar{\mu}\ell_o}{2} \right) - (1 + \gamma^2) \frac{\bar{\mu}^2 \ell_o^2}{4} - \frac{\rho}{\rho_{\text{crit}}} \right) + O(v^{-3}) \end{aligned} \quad (6.9)$$

where ρ denotes the eigenvalues of the energy density operator $\hat{\rho} \equiv \widehat{p_\phi^2/|p|}$ and as in the $k=0$ case we have set $\rho_{\text{crit}} = 3/(16\pi^2\gamma^3 G^2 \hbar) \approx 0.82\rho_{\text{Pl}}$. Although for brevity we have kept the sine functions in this equation, since $v^{-1} \sim \bar{\mu}^3$, to the leading order considered here one only needs to keep terms $O(\bar{\mu}^8)$ in their Taylor expansions. Finally, note that on substituting $\ell_o = 0$ in (6.9), we immediately obtain the effective Friedmann equation of [3] for the $k=0$ model.

To probe the possible turning points, it is useful to rewrite the modified Friedmann equation (6.9) in the following form

$$H^2 = \frac{8\pi G}{3} (\rho - \rho_1) \left(\frac{1}{\rho_{\text{crit}}} (\rho_2 - \rho) \right) + O(v^{-3}) \quad (6.10)$$

with,

$$\rho_1(v) = -\frac{3}{8\pi G} \frac{1}{\gamma^2 \bar{\mu}^2} \left(\frac{8\pi\gamma\ell_{\text{Pl}}^2}{6} \right)^{-1} \left(\frac{K}{|v|} \right)^{2/3} \left(\sin^2 \left(\frac{\bar{\mu}\ell_o}{2} \right) - (1 + \gamma^2) \frac{\bar{\mu}^2 \ell_o^2}{4} \right) \quad (6.11)$$

and

$$\rho_2(v) = \rho_{\text{crit}} \left(1 - \sin^2 \left(\frac{\bar{\mu}\ell_o}{2} \right) - (1 + \gamma^2) \frac{\bar{\mu}^2 \ell_o^2}{4} \right). \quad (6.12)$$

Note that while ρ_{crit} is a constant, ρ_1, ρ_2 are functions of v (and ρ is a function of v, p_ϕ). Along each dynamical solution of the effective evolution equations (6.3) and (6.4), ρ, ρ_1, ρ_2 all evolve. In the effective dynamics, along any given dynamical trajectory turning points occur when $\rho = \rho_1$ or $\rho = \rho_2$. Plots of solutions to the effective equations show that the classical recollapse occurs when $\rho = \rho_1$, where the universe reaches its maximum radius a_{max} and minimum density ρ_{min} , and the quantum bounce occurs when $\rho = \rho_2$ where the universe reaches its minimum radius a_{min} and maximum density ρ_{max} . Now, an examination of the

expressions of ρ_1 and ρ_2 show

$$\rho_{\min} := \rho_1|_{a=a_{\max}} = \frac{3}{8\pi G a_{\max}^2} \left(1 + O\left(\frac{\ell_{\text{Pl}}^4}{a_{\max}^4}\right) \right) \quad \text{and} \quad \rho_{\max} := \rho_2|_{a=a_{\min}} = \rho_{\text{crit}} \left(1 + O\left(\frac{\ell_{\text{Pl}}^2}{a_{\min}^2}\right) \right). \quad (6.13)$$

Numerical simulations showed that our notion of ‘semi-classicality at late times’ is surprisingly weak. For example, in the simulation with $p_\phi \approx 5 \times 10^3 \hbar$ (in the classical units $c=G=1$), the universe grows only to a maximum radius of $\approx 23\ell_{\text{Pl}}$ before undergoing the classical recollapse. Even for this small universe, effective equations predict that the density ρ_{\min} at the recollapse should agree with the classical Friedmann formula $\rho_{\min} = 3/8\pi G a_{\max}^2$ to one part in 10^{-5} and the density ρ_{\max} at the quantum bounce would equal the critical density ρ_{crit} —the density at the bounce in the $k=0$ models— to within a couple of percent. *These predictions are borne out in the numerical simulations of the exact LQC equations.* Since a_{\max} scales as $(p_\phi)^{1/2}$ and a_{\min} as $(p_\phi)^{1/3}$, effective equations imply that both approximations improve as p_ϕ increases and become almost exact for universes which grow to interesting macroscopic sizes.

In particular, as one would hope, the effective theory accurately reproduces the predictions of classical general relativity in the low curvature regime. Yet, already the leading order correction from quantum geometry is strong enough to resolve singularities and replace them with a bounce. It is also noteworthy that for universes which grow to large macroscopic sizes, the density at the quantum bounce is universal, and equals that in the $k=0$ models. These general features represent key predictions of the numerical evolution of the full quantum equations. The effective theory provides a physical understanding of how they come about. In particular it shows that the most important corrections come from the gravitational part of the quantum Hamiltonian constraint. Indeed, since we need only the leading, classical part of $B(v)$ in this analysis, the quantum modifications of the matter Hamiltonian play no role in the leading order corrections discussed here.

In the last part of our above discussion we have ignored terms $O(v^{-3})$. A priori it is possible that the sum of these terms is not negligible and could even dominate the leading term. However, a comparison with numerical simulations shows that the predictions obtained from just the leading order quantum corrections in the effective theory accurately describe the full quantum dynamics of states which are semi-classical at late times and the accuracy improves as p_ϕ increases. Thus, although one could not draw definitive conclusions just from effective equations, when used in conjunction with numerical simulations, they provide an easily manageable and powerful tool to probe quantum geometry effects for universes which grow to $a_{\max} \sim 25\ell_{\text{Pl}}$ or more.

B. Results

Main results on quantum dynamics can be summarized as follows.

1. Consider a classical solution which evolves from the big-bang to the big crunch, reaching a large maximum radius a_{\max} . Fix a point on this trajectory where the universe has reached macroscopic size and consider a semi-classical state peaked at this point (see section V B). Such states remain sharply peaked throughout the given ‘cycle’, i.e., from the quantum bounce near the classical big-bang to the quantum bounce near the classical big-crunch. The notion of semi-classicality used here is rather weak: these

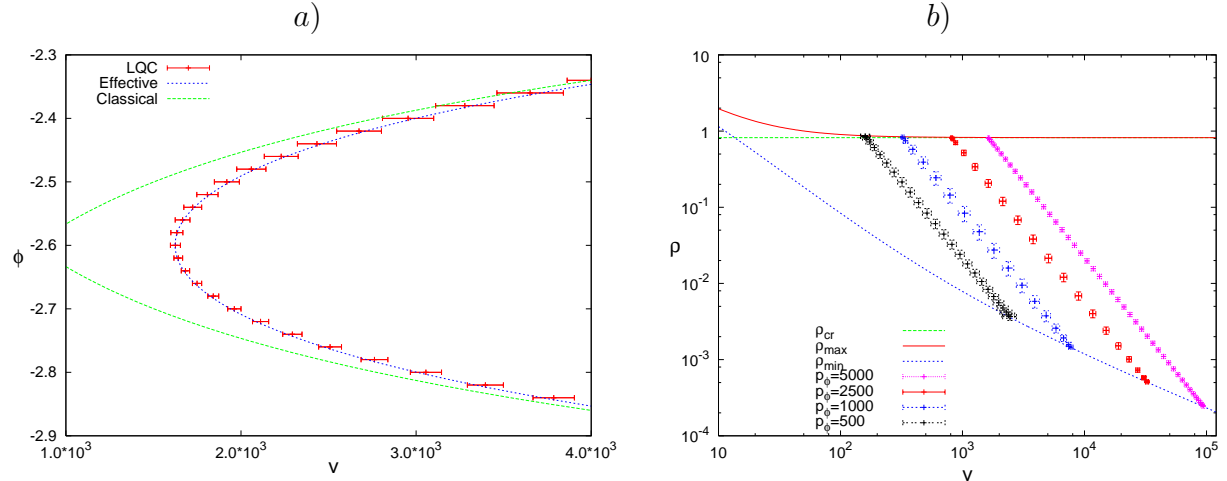


FIG. 7: a) Zoom on the portion near the bounce point of comparison between the expectation values and dispersion of $\hat{v}|_\phi$, the classical trajectory and the solution to effective dynamics. At large values of $|v|_\phi$ the classical trajectory approaches the quantum evolution. Values of parameters are the same as in Fig. 6. b) The behavior of expectation values of $\hat{\rho}$ for different values of p_ϕ^* are shown. On each solution, these are bounded between a ρ_{max} and a ρ_{min} . For a universe peaked at large values of p_ϕ , $\rho_{max} \approx \rho_{crit}$.

results hold even for universes with $a_{max} \approx 25\ell_{Pl}$ and the ‘sharply peaked’ property improves as a_{max} grows.

2. The trajectory defined by the expectation values of the Dirac observable $\hat{v}|_\phi$ in the full quantum theory is in good agreement with the trajectory defined by the classical Friedmann dynamics until the energy density of the scalar field becomes comparable to the maximum energy density $\rho_{max} \sim \rho_{crit} \approx 0.82\rho_{Pl}$. Then the classical trajectory deviates from the quantum evolution. In the classical solution, the matter energy density keeps increasing on further evolution, eventually leading to a big bang (respectively, big crunch) singularity in the backward (respectively, forward) evolution, when $v \rightarrow 0$. The situation is very different with quantum evolution. Now the universe bounces at $\rho = \rho_{max}$, avoiding the past (or the big bang) and future (or the big crunch) singularities.
3. The expectation values and relative dispersions of \hat{p}_ϕ remain constant during different stages of evolution. Thus the expanding and contracting branches correspond to the same value of $\langle \hat{p}_\phi \rangle$. Further, as a check on numerics we verified that the norm of the states is also preserved during the entire evolution.
4. After the quantum bounce the energy density of the universe decreases and, when $\rho \ll \rho_{max}$, the quantum evolution is well-approximated by the classical trajectory. On subsequent evolution, the universe recollapses both in classical and quantum theory at the value $v = v_{max}$ when energy density reaches a minimum value ρ_{min} .
5. The trajectory obtained from effective Friedmann dynamics (6.9) is in excellent agreement with quantum dynamics *throughout the evolution*. (See Figs. 6 and 7a.) In

particular, the maximum and minimum energy densities predicted by the effective description agree with the corresponding expectation values of the density operator $\hat{\rho} \equiv \widehat{p_\phi^2/|p|^3}$ computed numerically. Evolution of the expectation values of $\hat{\rho}$ with $|v|_\phi$ is shown in Fig. 7b.

6. For quantum states under discussion, the density ρ_{\max} is well approximated by $\rho_{\text{crit}} \approx 0.82\rho_{\text{Pl}}$ up to terms $O(\ell_{\text{Pl}}^2/a_{\min}^2)$, independently of the details of the state and values of p_ϕ . (For a universe with maximum radius of a megaparsec, $\ell_{\text{Pl}}^2/a_{\min}^2 \approx 10^{-76}$.) The density ρ_{\min} at the recollapse point also agrees with the value $(3/(8\pi G a_{\max}^2))$ predicted by the classical evolution to terms of the order $O(\ell_{\text{Pl}}^4/a_{\max}^4)$. Furthermore the scale factor a_{\max} at which recollapse occurs in the quantum theory agrees to a very good precision with the one predicted by the classical dynamics.
7. The relative dispersion of $|v|_\phi$ increases —but very slowly —as one evolves through many cycles. Effective Friedmann dynamics provides insight into this behavior of the quantum state. Let us first consider two nearby solutions to the effective equation with slightly different p_ϕ but with same value of v at a chosen $\phi = \phi_o$. Then the relative difference between v of the two solutions after one cycle can be estimated using Eqs.(6.3) and (6.4) as

$$\frac{\delta v}{v} \approx \sqrt{48\pi^3 G} \alpha \frac{\delta p_\phi}{p_\phi} \quad (6.14)$$

where δp_ϕ is the difference between values of p_ϕ of the two effective trajectories and $\sqrt{G}\alpha = 0.0259272 \pm (5 \times 10^{-7})$ (see 5.3). This estimate was found to provide a good upper bound on the relative dispersions computed using numerical evolution of the quantum state.

8. The state remains sharply peaked for a *very large number of ‘cycles’*. This number can be estimated using Eq.(6.14). Consider the example of a semi-classical state with an almost equal relative dispersion in p_ϕ and $|v|_\phi$ and peaked at a large classical universe of the size of a megaparsec. When evolved, it remains sharply peaked with relative dispersion in $|v|_\phi$ of the order of 10^{-6} *even after 10^{50} cycles of contraction and expansion!* Any given quantum state eventually ceases to be sharply peaked in $|v|_\phi$ (although it continues to be sharply peaked in p_ϕ). Nonetheless, the quantum evolution continues to be deterministic and well-defined for infinite cycles, i.e., on the entire real line of the emergent time ϕ . This is in sharp contrast with the classical theory where the equations break down at singularities and there is no deterministic evolution from one cycle to the next. In this sense, in LQC the $k=1$ universe is *cyclic*, devoid of singularities. As in the $k=0$ case, this non-singular evolution holds for all states, not just the ones which are semi-classical at late times. There is no fine tuning of initial conditions. Also, there is no violation of energy conditions. Indeed, as discussed in section VIA, quantum corrections to the matter Hamiltonian do not play any role in the resolution of the singularity. The standard singularity theorems are evaded because the geometrical side of the classical Einstein’s equations is modified by the quantum geometry corrections of LQC.
9. In the $k=1$ model, certain effective equations have been written down and used to predict non-singular bounces [29] in the broad framework of LQC. The presence of

these bounces was also used to study the onset of a successful period of inflation in closed models [30]. How do these analysis compare with that presented in this paper? There are two important differences. First, these works focused on the matter part of the Hamiltonian constraint and made a crucial use of quantum corrections to the matter Hamiltonian arising from the use of representations (of $SU(2)$ -holonomies) labeled by large values of j . Second, these large j representations were used only in the matter part of the Hamiltonian and not in the gravitational part. Since then Perez [17] has shown that mathematical consistency requires us to use the $j = 1/2$ representation in 3-dimensional gravity. He also argues that the same should hold in 4 dimensions. In any case, while the use of, say $j = 1$ representation could be justified because the model has no spinor fields, the use of large j values appears to be unnatural and needs an independent justification which is still lacking. Similarly, without an independent justification, an asymmetric treatment of the gravitational and matter appears to be ad-hoc [16], somewhat similar to using two different metrics on the right and left hand side of classical Einstein's equations. Our analysis used the fundamental, $j = 1/2$ representation for geometry as well as matter. Our numerical simulations as well as effective equations show that with this choice the modifications of the matter Hamiltonian play no role. This is consistent with findings in the older literature; indeed this is the reason why large j values were used there. In our analysis, it is the modification of the gravitational part of the Hamiltonian constraint that plays a key role in the singularity resolution. In the older literature, by contrast, these modifications were ignored. Nonetheless, basic physical ideas in these older works are intriguing and it would be interesting to reanalyze those issues using the Hamiltonian constraint introduced in this paper.

We will conclude this section by clarifying two issues that have arisen from a recent work [11] addressed to computational physicists, particularly numerical relativists. Although this discussion refers only to the $k=0$ model considered in [1–3], it is included here because the same issues can arise in the $k=1$ model.

The phrase “These bounces can be understood as spurious reflections” in the abstract (and again in the body) of [11] was interpreted by some as suggesting that the bounces reported in [1–3] were artifacts of bad numerics. This is certainly *not* the case: Not only were those simulations performed with all the due care but our result that the LQC equations predict a genuine, physical bounce was in fact reproduced in the first half of [11]. Indeed, this part is a nice summary of our numerical results geared to computational physicists. From discussions with the author we understand that the intent of that phrase was to say: ‘had the physical problem been to solve a wave equation in the *continuum* and had one used non-uniform grids, one would also have found bounces which, from the perspective of continuum physics of this hypothetical problem, would be interpreted as spurious reflections in finite difference discretizations’. This is likely to be an illuminating point for computational physicists but is not physically relevant in LQC where the basic equation is a difference equation.

The second part of the paper considers a modification of the quantum Hamiltonian constraint by “adding ad-hoc higher order terms.” It is then suggested that such modifications could remove the bounce. Let us analyze the issue from a mathematical perspective even though the analysis and conclusions have no obvious physical significance since the modifications do not result from any systematic, physical considerations. Then, since the physical state is symmetric under orientation reversal, simulations reported in [11] imply that the

bounce would *not* disappear but change its character. In the *physical* solution there would again be a pre-big-bang, contracting branch which would be joined in a deterministic fashion to a post-big-bang expanding branch. However, now the two branches will meet at $v = 0$. Although the ensuing differences are not trivial, the qualitative picture is not changed even by these ad-hoc modifications.⁹

VII. DISCUSSION

A. Key Features

Key features of the $k=1$ model can be summarized as follows.

i) The scalar field ϕ serves as emergent time at all three levels: classical general relativity, WDW theory and LQC. In the classical theory, every solution undergoes a recollapse but ϕ remains single valued. Each solution begins with a big bang and ends with a big crunch and ϕ ranges over the entire real line irrespective of the constant of motion p_ϕ . In the WDW theory and LQC the form of the Hamiltonian constraint operator implies that ϕ can serve as emergent time also in the quantum theory. Situation with the range of ϕ in the WDW theory is the same as that in classical general relativity since the singularities are not resolved, i.e., since quantum dynamics can not unambiguously evolve the state across these singularities. In LQC on the other hand the singularities *are* resolved and the quantum evolution across the putative classical singularities is deterministic. The range of ϕ continues to be the entire real line.

ii) In LQC, three sets of results show that the big bang and the big-crunch singularities are both resolved. First, the LQC effective equations do not break down. Rather, while the classical Friedmann equation has only one root at which $H^2 = (\dot{a}/a)^2$ vanishes, quantum corrections introduce a second root when the matter density enters the Planck regime, altering classical dynamics and giving rise to bounces. The second result refers to full quantum dynamics: in contrast to the WDW theory, in LQC *every* state in \mathcal{H}_{phy} has a well-defined unitary evolution for the full range $(-\infty, \infty)$ of the ‘emergent time’ ϕ . The third set of results is more detailed. It again involves the full dynamics of LQC but only semi-classical states in \mathcal{H}_{phy} . Consider a classical trajectory in the v - ϕ plane in which the universe evolves to a macroscopic maximum size. The classical Friedmann equation implies that the universe attains its maximum volume V_{max} at the recollapse point and this value is related to the constant of motion p_ϕ via¹⁰

$$V_{\text{max}} = (16\pi G/3\ell_o^2)^{\frac{3}{4}} p_\phi^{\frac{3}{2}} \approx 0.6 p_\phi^{\frac{3}{2}}. \quad (7.1)$$

Hence, in the solution under consideration p_ϕ has to be large. Consider a point on this classical trajectory at a late time when the volume is macroscopic and a semi-classical state

⁹ Indeed, as the numerical simulations of [2, 3] show, the ‘reflection’ and transmission’ phenomenon discussed in the second part of [11] occurs even in standard LQC. It does not have deep physical significance in the final picture because physical states are symmetric under the orientation reversal map Π .

¹⁰ Here and in what follows, numerical values are given in the classical units $G=c=1$. In these units p_ϕ has the same physical dimensions as \hbar and the numerical value of \hbar is $2.5 \times 10^{-66} \text{cm}^2$.

in which Dirac observables \hat{p}_ϕ and $|\hat{v}|_{\phi_o}$ are peaked at this point at ‘time’ $\phi = \phi_o$. When evolved, this quantum state remains semi-classical, sharply peaked at the classical solution under consideration during the entire cycle, except near the big-bang and the big-crunch. There, because of repulsive effects of quantum geometry, the wave function bounces when the peak reaches a minimum volume:

$$V_{\min} = \left(\frac{4\pi G \gamma^2 \Delta}{3} \right)^{\frac{1}{2}} p_\phi \approx (1.28 \times 10^{-33} \text{ cm}) p_\phi \quad (7.2)$$

Thus, the wave function does not enter a neighborhood of the classical singularity. The size of this neighborhood is dictated by the value of the constant of motion p_ϕ and can be *much* larger than the Planck size. Finally, note that in the mathematical limit in which the area gap Δ is taken to zero, V_{\min} vanishes. More generally, this is also the limit in which LQC reduces to the WDW theory. Thus, one can use Δ as a knob to turn on or off quantum geometry effects and understand the ‘mechanism’ behind the singularity resolution.

iii) To better understand the physical conditions at the quantum bounce, let us consider a couple of examples. Consider first a quantum state describing a universe which attains a maximum radius of a megaparsec. Then the quantum bounce occurs when the volume reaches the value $V_{\min} \approx 5.7 \times 10^{16} \text{ cm}^3$, *some 10^{115} times the Planck volume*. As a second illustration, consider a semi-classical state representing a large universe whose density at the classical re-collapse is about the current density of our universe $\rho \approx 9.7 \times 10^{-30} \text{ gm/cc}$. Then, the quantum bounce would occur at $V_{\min} \approx 1.4 \times 10^{24} \text{ cm}^3$. Thus the ‘quantum’ or the ‘Planck’ regime is defined not by the volume of the universe but by the value of the matter density, or space-time curvature. In universes which grow to large macroscopic sizes, these quantities can attain Planck scale even when the volume of the universe is large. Figures quoted above were arrived at using our model where the scalar field is massless. The presence of potentials could significantly modify their values. Still, since the values of V_{\min} are so huge, these considerations are useful in drawing qualitative conclusions. For example, they suggest that in universes which grow to macroscopic sizes, the so called ‘ d_j -effects’ associated with modifications of the matter Hamiltonians due to quantum geometry will not be dynamically significant in homogeneous models (unless one considers astronomically large—and hence implausible—values of j).

iv) Since detailed predictions were obtained only for states which are semi-classical at late times, it is interesting to ask *how* semi-classical these states have to be. How quantum mechanical can we make the parameters of the universe, still keeping the quantum state semi-classical in the sense used in this paper? The typical values of p_ϕ used in the simulations reported in section V was $5 \times 10^3 \ell_{\text{Pl}}^2$. These universes evolve only to a maximum volume of $V_{\max} \approx 2.3 \times 10^5 \ell_{\text{Pl}}^3$ before undergoing a recollapse. *Results of our numerical simulations show that the necessary semi-classical considerations hold already for such small universes*. In particular, the maximum value ρ_{\max} of the matter density is well approximated by the critical value $\rho_{\text{crit}} = 0.82 \rho_{\text{Pl}}$ already for these universes. A combination of numerics and effective-equations shows that the approximation becomes increasingly better as one considers larger and larger universes. Similarly, our numerical results have shown that the recollapse occurs at the classically predicted values already for these universes. In these cases, the matter density even at the recollapse point is quite high, approximately $2.2 \times 10^{-4} \rho_{\text{Pl}}$. Thus, several interesting phenomena occur in a rather small interval (of just four to five orders of magnitude) of density and volume. As our detailed plots show, there is a very narrow range of these parameters in which quantum geometry effects become significant. They

grow extremely quickly, overwhelm the classical attractive force, cause the bounce and then become insignificant very quickly again.

v) We would like to emphasize that while quantum geometry effects resolve classical singularities, we did not predict the emergence of classicality at late times within any given cycle.¹¹ These two issues are logically distinct. Indeed, in our detailed analysis we simply restricted ourselves to a single cycle and to states which are semi-classical at late times therein. At first, it may appear that the problem of actually specifying such states would be impossibly difficult in more realistic models since such specification would have to incorporate all the complexities that have developed during the epoch during which the universe grew to a macroscopic size. However, as discussed above, this ‘macroscopic size’ can be very small and the required specification of a semi-classical state could be done at a relatively early time before complicated structures develop. For example, in an inflationary scenario one could specify the state immediately after the end of inflation, or perhaps even before the onset of inflation since, in the current observationally favored scenarios, matter density is significantly smaller than the Planck density even at the onset. Thus, while the conceptual issue of singling out a preferred family of states using general principles remains largely unexplored, there do not appear to be any ‘practical’ difficulties in specifying the state.

vi) Since both the big bang and the big crunch singularities are resolved, the quantum wave function evolves through *infinitely many* classical cycles. Thus, in the $k=1$ model, the quantum space-time of LQG is vastly larger than that the classical space-time of general relativity. The issue of emergence of semi-classicality raised above can now be elevated to the *infinite* history of the quantum universe. Let us then begin a classical solution in which the maximum volume of the universe is large, say more than a megaparsec, and consider a quantum state which is peaked at a point on this classical trajectory at a late ‘time’, $\phi = \phi_o$. As discussed in section VI, this state has interesting properties. Except near the classical singularities, it will remain sharply peaked not only on the given classical solution during its cycle but also for over 10^{50} cycles resulting from quantum bounces. However, because the eigenvalues of $-i\partial_\phi \equiv \sqrt{\Theta}$ are not exactly evenly spaced, eventually the wave function will spread and cease to be semi-classical. The issue of converse is intriguing. Consider any state which is sharply peaked at a large value of the constant of motion \hat{p}_ϕ but has a large spread for the volume operator $|\hat{v}|_\phi$ at the initial instant of ‘time’ $\phi = \phi_o$. Initially, such a state is not semi-classical. However, would the LQC dynamics evolve it to a state which is eventually sharply peaked at a classical trajectory? The answer appears to be in the affirmative [31]. If so, all states which are peaked at a very large value of p_ϕ would eventually become semi-classical. In this precise sense, semi-classicality would be generic.

B. Classical recollapse from LQC

As discussed in section I, a major challenge to any background independent quantum gravity approach, such as LQG, is to ensure that there is a sufficiently large semi-classical sector. LQC offers a non-trivial context to probe this issue. Are the quantum geometry effects subtle enough to dominate near classical singularities but turn themselves off on

¹¹ As discussed in the last section of [2], the bounce picture has a suggestive, intriguing relation to the Hartle-Hawking [23] proposal for the wave function of the universe. It may well suggest an avenue to address this issue.

large scales? As results of [2] show, this is a delicate issue. Indeed, the evolution generated by the Hamiltonian constraint that was generally used in LQC until recently (the so-called ‘ μ_o -evolution’), the answer was in the negative. Certain quantum effects associated with that evolution could alter the classical predictions even in regimes in which the matter densities and space-time curvatures are completely tame. In the $k=0$ case, this severe drawback was overcome by the ‘improved dynamics’ of [3].

In the $k=1$ models, the classical recollapse provides an excellent venue to test semi-classical viability because, as the analysis of section VI shows, both the classical recollapse and the quantum bounce are governed by the same condition: the vanishing of $H^2 = (\dot{a}/a)^2$. For the recollapse, an agreement with the classical theory requires that quantum geometry effects be negligible while the bounce can occur only if these effects dominate. At first sight then there appears to be a tension. In [6], Green and Unruh analyzed this issue numerically in the same model as the one considered in this paper and concluded that the tension is real. More precisely, they used *the then available* Hamiltonian constraint of LQC [5] and found numerical evidence against the occurrence of recollapse. For large universes, the classical recollapse occurs when matter density and space-time curvatures are very small compared to the Planck scale. Therefore, a theory in which recollapse does not occur would contradict classical general relativity in a domain where there is every reason to expect its validity. Although Green and Unruh did not have access to a physical inner product or observables to arrive at a definitive interpretation of their results, they concluded that it is unlikely that one could find an interpretation in which such large deviations from the classical theory are appropriate.

In this paper we have overcome important limitations pointed out by Green and Unruh, thereby completing the LQC program. We found that LQC does predict a recollapse and, furthermore, it occurs at the values of matter density and volume predicted by the classical theory. How did this strikingly different conclusion come about? We will conclude by first summarizing how the general criticisms of [6] were addressed and then discussing the issue of the recollapse.

i) General Framework: Green and Unruh began by pointing out that much of the then successes of LQC arose from effective equations and the interpretation of quantum states had remained unclear because the physical inner product and observables had not been specified. They pointed out that, in particular, the issue of time had not been addressed explicitly and the implicit use of the scale factor as time has obvious problems in the $k=1$ model. In this paper we showed that the use of the scalar field as emergent time is free of the difficulties associated with the multi-valued character of the scale factor in closed models. We constructed the physical sector of LQC in detail, including the physical inner product, Dirac observables and well-controlled semi-classical states. We then numerically solved the Hamiltonian constraint and calculated the expectation values and fluctuations of Dirac observables. In particular, we analyzed dynamics in full LQC, not in just in an effective approximation.

ii) Recollapse: Our Hamiltonian constraint is quite different from that used in [6]. Thus, the very starting points of the two sets of numerical simulations are distinct. In particular, while \hat{C}_{grav} used in [6] was *not self-adjoint*, ours is. This has two consequences. First, since our operator Θ is self-adjoint on $\mathcal{H}_{\text{kin}}^{\text{grav}}$ and we are guaranteed that it admits a complete set of eigenfunctions. Furthermore since its spectrum is discrete [10] the eigenfunctions in the spectral family are normalizable. This immediately implies that they must decay for large $|v|$. Our numerical simulations showed that the decay is exponential for large $|v|$, which ensured

that physically appropriate wave packets would exhibit a recollapse. The numerical task of actually finding these eigenfunctions was delicate because the normalizable ones constitute a set of ‘zero measure’ among all eigenfunctions, i.e., because ‘most’ eigenfunctions diverge in at least one of the two asymptotic regimes $v \rightarrow \pm\infty$. However, because Θ is self-adjoint with appropriate properties, the existence of these eigenfunctions was ensured from the beginning. This was not the case for the analysis of [6]. Indeed the principal argument there was that the authors found only exponentially growing eigenfunctions, signaling absence of recollapse. Secondly, for reasons discussed in Sec.I, it was important that we used the ‘improved dynamics’ of [3] (rather than the older, ‘ μ_o evolution’). Finally, the effective-equation-analysis shows how LQC manages to have both the quantum bounce and the classical recollapse. For, the modified Friedmann equation now has two roots: one a la classical general relativity at a low density causing the recollapse, and a *new one* near Planck density causing the bounce. The quantum geometry effects are small at the old, classical root but cause and thus dominate the new root.

Acknowledgments: We would like to thank Golam Hossain and Pablo Laguna for discussions, Eloisa Bentivegna for her help in calculating the Bessel functions of section III and participants of the 11th Marcel Grossmann conference and the Unruh-Wald fest for interesting comments and suggestions. This work was supported in part by the NSF grant PHY-0456913, the Alexander von Humboldt Foundation, the Kramers Chair program of the University of Utrecht, the Eberly research funds of Penn State and the Marie Curie Incoming International Fellowship MIF1-CT-2006-022239 to KV.

APPENDIX A: INVARIANT FRAMES, EXPLICIT CHARTS AND HOLONOMY

In this appendix we spell out conventions on the fiducial structures that are used in the main body of the paper and provide an explicit calculation of holonomy used in the definition of the Hamiltonian constraint. The discussion on conventions is somewhat detailed because there has been some confusion due to unfortunate typos in some of the standard literature on homogeneous cosmologies.

1. Invariant frames

In the $k=1$ case the underlying, spatial 3-manifold M is a 3-sphere \mathbb{S}^3 . It is often convenient to identify it with the symmetry group $SU(2)$ which acts on it simply and transitively. In what follows we will generally do so. Let us denote the symmetry vector fields on M by ξ_i^a . All homogeneous isotropic tensor fields on M are invariant under diffeomorphisms generated by ξ_i^a . In particular, these vector fields are the Killing vectors of all 3-metrics considered in this paper.

Let us fix a basis τ^i in the Lie algebra $\mathfrak{su}(2)$, satisfying $\tau^i \tau^j = \frac{1}{2} \epsilon^{ij}_k \tau^k - \frac{1}{4} \delta^{ij} \mathbb{I}$ and denote by k_{ij} the metric on $\mathfrak{su}(2)$ for which these τ^i constitute an orthonormal basis. In what follows the ‘internal’ or Lie-algebra indices will be lowered and raised using k_{ij} and its inverse k^{ij} . It follows in particular that $\epsilon_{ijk} := \epsilon^{mn}_k q_{mi} q_{jn}$ is a 3-form on $\mathfrak{su}(2)$ satisfying $\epsilon_{ijk} \epsilon^{ijk} = 6$.

Recall that $SU(2)$ admits a natural, left invariant, Lie-algebra valued, Cartan 1-form $\omega = g^{-1}dg$. It naturally defines a co-frame ${}^o\omega_a^i$ on M via:

$$g^{-1}dg =: {}^o\omega = {}^o\omega^i \tau_i \tag{A1}$$

We will denote the dual frame by ${}^o e_i^a$; thus ${}^o e_i^a {}^o \omega_a^j = \delta_i^j$ and ${}^o e_i^a {}^o \omega_b^i = \delta_b^a$. From the definition of the natural left-invariant 1-form ω it follows that the co-frames ${}^o \omega_a^i$ and the frames ${}^o e_i^a$ satisfy the relations:

$$d{}^o \omega^i + \frac{1}{2} \epsilon_{jk}^i {}^o \omega^j \wedge {}^o \omega^k \quad \text{and} \quad [{}^o e_i, {}^o e_j] = \epsilon_{ij}^k {}^o e_k \quad (\text{A2})$$

These will be our fiducial co-frames and frames on M . The 1-forms ${}^o \omega_a^i$ and the vector fields ${}^o e_i^a$ are left invariant. Thus ξ_i^a , the infinitesimal generators of left translations, Lie drag these fields:

$$\mathcal{L}_{\xi_i} {}^o \omega^j = 0, \quad \mathcal{L}_{\xi_i} {}^o e_j = 0 \quad (\text{A3})$$

and satisfy the $\mathfrak{su}(2)$ commutation relations $[\xi_i, \xi_j] = \epsilon_{ij}^k \xi_k$. The metric

$${}^o q_{ab} := {}^o \omega_a^i {}^o \omega_b^j k_{ij} \quad (\text{A4})$$

on M will serve as the fiducial metric on M . By inspection ξ_i^a are Killing fields of ${}^o q_{ab}$. Since they act simply and transitively on M , it follows that ${}^o q_{ab}$ is of constant curvature. *However, in contrast to one's initial expectations, it is the metric on a 3-sphere of radius $a = 2$ (rather than $a = 1$).*¹²

The volume of M with respect to ${}^o q_{ab}$ is $V_o = 2\pi^2 a^3 = 16\pi^2$ and its scalar curvature is ${}^o R = 6/a^2 = 3/2$. *It will be convenient for us to use the symbol V_o (rather than the numerical value $16\pi^2$) to denote the fiducial volume of M . We will also set $\ell_o = V_o^{1/3}$.* In the standard charts used in textbooks, the components of ${}^o q_{ab}$ can be expressed as:

$$\begin{aligned} ds_o^2 &= a^2 [d\chi^2 + \sin^2 \chi (d\theta^2 + \sin^2 \theta d\varphi^2)] \\ &= a^2 \left[\frac{dr^2}{1-r^2} + r^2 (d\theta^2 + \sin^2 \theta d\varphi^2) \right] \end{aligned} \quad (\text{A5})$$

with $a = 2$, where $\chi, \theta \in (0, \pi)$, $\phi \in (0, 2\pi)$ and $r = \sin \chi \in (0, 1)$.

Finally, the fact that the choice $a = 2$ in the fiducial metric is geometrically natural can also be seen directly in terms of 3-sphere geometries without reference to $\text{SU}(2)$ and the natural Cartan form thereon. Consider the Euclidean metric and 3-spheres $\mathbb{S}_{(a)}$ of radius a on \mathbb{R}^4 . The natural action of the rotation group $\text{SO}(4)$ on \mathbb{R}^4 leaves each $\mathbb{S}_{(a)}$ invariant. It is the isometry group of the intrinsic metric on $\mathbb{S}_{(a)}$. These six Killing fields can be naturally divided into two $\text{SO}(3)$ sub-Lie-algebras (resulting from self-dual and anti-self-dual 2-forms on \mathbb{R}^4). These are the right and left rotations and all three right rotations commute with all three left. In the natural chart x, y, z, w on \mathbb{R}^4 , these six Killing fields K_i^\pm can be expressed

¹² This normalization is fixed by our choice that the natural left invariant 1-forms ${}^o \omega_a^i$ be orthonormal. In the frame formalism it would be awkward and geometrically unnatural to work with rescaled ${}^o \omega_a^i$. If one is interested only in metrics and not frames, on the other hand, one can just as easily work with a unit 3-sphere. This is the usual choice in geometrodynamics. In the literature on cosmology the fiducial metric is sometimes chosen to have unit *scalar curvature* ${}^o R$ rather than unit radius; then the 3-sphere radius is $a = 1/\sqrt{6}$.

as:

$$\begin{aligned} K_1^\pm &= \frac{1}{2} (x\partial_y - y\partial_x \pm z\partial_w \mp w\partial_z) \\ K_2^\pm &= \frac{1}{2} (w\partial_x - x\partial_w \pm z\partial_y \mp y\partial_z) \\ K_3^\pm &= \frac{1}{2} (y\partial_w - w\partial_y \pm z\partial_x \mp x\partial_z) \end{aligned} \quad (\text{A6})$$

so that $[K_i^\pm, K_j^\pm] = \epsilon_{ij}^{k} K_k^\pm$ and $[K_i^+, K_j^-] = 0$. Note that because of the first set of commutation relations, we do not have the freedom to rescale the K_i^\pm by a constant. The three vectors K_i^\pm in each set are mutually orthogonal. Now we can ask: On which \mathbb{S}^3 is this basis orthonormal? The answer is: the 3-sphere with radius $a = 2$. On M , these are the basis $\{^o e_i^a\}$ and $\{\xi_i^a\}$.

2. An explicit chart

In the textbook treatments of $\text{SU}(2)$, its elements are often written as 2×2 matrices:

$$g = \begin{pmatrix} a & -b \\ b^\star & a^\star \end{pmatrix} \quad \text{where} \quad \begin{aligned} a &= e^{\frac{i}{2}(\alpha+\gamma)} \cos(\beta/2) \\ b &= e^{-\frac{i}{2}(\alpha-\gamma)} \sin(\beta/2) \end{aligned} \quad (\text{A7})$$

where $0 \leq \alpha < 2\pi$, $0 \leq \beta \leq \pi$ and $0 \leq \gamma < 4\pi$. (The ranges of α and γ can be interchanged.) As is usual with angular coordinates, this chart breaks down at the poles $\alpha = 0, \beta = 0, \gamma = 0$ (which corresponds to the identity, \mathbb{I}) and $\alpha = 0, \beta = \pi, \gamma = 0$ (which corresponds to $-\mathbb{I}$). Nonetheless, as with the standard spherical polar coordinates, this chart is convenient for explicit calculations.

In this chart, the left invariant co-frame ${}^o\omega_a^i$ can be expressed as:

$$\begin{aligned} {}^o\omega^1 &= -\cos\gamma d\beta - \sin\gamma \sin\beta d\alpha \\ {}^o\omega^2 &= \sin\gamma d\beta - \cos\gamma \sin\beta d\alpha \\ {}^o\omega^3 &= d\gamma + \cos\beta d\alpha \end{aligned} \quad (\text{A8})$$

and the left invariant frame e_i^a as

$$\begin{aligned} {}^o e_1 &= -\cos\gamma \frac{\partial}{\partial\beta} - \frac{\sin\gamma}{\sin\beta} \frac{\partial}{\partial\alpha} + \frac{\cos\beta \sin\gamma}{\sin\beta} \frac{\partial}{\partial\gamma} \\ {}^o e_2 &= \sin\gamma \frac{\partial}{\partial\beta} - \frac{\cos\gamma}{\cos\beta} \frac{\partial}{\partial\alpha} + \frac{\cos\beta \cos\gamma}{\sin\beta} \frac{\partial}{\partial\gamma} \\ {}^o e_3 &= \frac{\partial}{\partial\gamma}. \end{aligned} \quad (\text{A9})$$

Finally the right invariant vector fields—which Lie drag our co-frame and the frame—are

given by:

$$\begin{aligned}
\xi_1 &= \cos \alpha \frac{\partial}{\partial \beta} - \frac{\cos \beta \cos \alpha}{\sin \beta} \frac{\partial}{\partial \alpha} + \frac{\sin \alpha}{\sin \beta} \frac{\partial}{\partial \gamma} \\
&= -[\cos \alpha \cos \gamma - \cos \beta \sin \alpha \sin \gamma]^o e_1 + [\cos \alpha \sin \gamma + \cos \beta \sin \alpha \cos \gamma]^o e_2 + [\sin \alpha \sin \beta]^o e_3 \\
\xi_2 &= \sin \alpha \frac{\partial}{\partial \beta} + \frac{\cos \beta \cos \alpha}{\sin \beta} \frac{\partial}{\partial \alpha} - \frac{\cos \alpha}{\sin \beta} \frac{\partial}{\partial \gamma} \\
&= -[\cos \gamma \sin \alpha + \cos \beta \cos \alpha \sin \gamma]^o e_1 + [\sin \alpha \sin \gamma - \cos \beta \cos \alpha \cos \gamma]^o e_2 - [\cos \alpha \sin \beta]^o e_3 \\
\xi_3 &= -\frac{\partial}{\partial \alpha} \\
&= \sin \beta \sin \gamma^o e_1 + \sin \beta \cos \gamma^o e_2 - \cos \beta^o e_3.
\end{aligned} \tag{A10}$$

Note that although the components of e_i^a and ξ_i^a diverge on the 2-torus $\beta = 0$, this is just an artifact of the failure of the chart there. All six vector fields are globally well-defined. In particular the expressions of ξ_i^a as linear combinations of e_i^a are globally well-behaved.

From the expression of the 1-forms ω_a^i we can readily compute the components of the fiducial metric:

$$dS_o^2 = d\alpha^2 + d\beta^2 + d\gamma^2 + 2d\alpha d\gamma \tag{A11}$$

The integral curves of the vector fields e_3^a (as well as ξ_3^a) are circles which provide a Hopf fibration of \mathbb{S}^3 . The quotient \hat{M} is topologically \mathbb{S}^2 with the induced metric

$$d\hat{s}^2 = d\beta^2 + \sin^2 \beta d\alpha^2 \tag{A12}$$

Thus β, α are the standard polar coordinates on the quotient \hat{M} and the induced metric on it is that of an *unit* 2-sphere.

3. Holonomy

The Hamiltonian constraint involves the field strength F_{ab}^k of the $SU(2)$ -connection

$$A_a^i := c^o \omega_a^i \tag{A13}$$

In LQG, there is no operator corresponding to the connection itself; only the holonomy operators are well-defined. Therefore, we need to express the field strength as an appropriate limit of a suitable holonomy [2, 3, 8]. Now in $k=0$ cosmologies, the right and left invariant vector fields on M coincide. Since they generate translations along the x, y, z directions, they commute. Hence to calculate the component $F_{32}^k := e_3^a e_2^b F_{ab}^k$ of the field strength, we can construct a square \square by moving along z and y directions a distance $\bar{\mu}$ (as measured by the fiducial metric q_{ab}), evaluate the holonomy along this loop, divide it by the area enclosed by the loop and take the limit as the loop shrinks. Because of homogeneity, F_{32}^k can be evaluated at any point of M and because of isotropy, F_{32}^k determines F_{ab}^k completely.

In the present $k=1$ case we wish to follow a similar procedure. Again, F_{32}^k can be evaluated at any point of M and fully determines F_{ab}^k . However, now the vector fields e_3^a and e_2^a do not commute. Therefore, as explained in the main text, we can not form the desired loop \square_{ij} by moving along 4 segments of their integral curves. However, since the left invariant vector fields e_i^a do commute with the right invariant vector fields ξ_i^a , we *can* construct the

desired closed loop \square_{ij} using integral curves of ${}^oe_i^a$ and ξ_j^a .

For definiteness, let us start with the point $(\alpha = 0, \beta = \pi/2, \gamma = 0)$. At this point, $\xi_3^a = -{}^oe_2^a$ and we can calculate the component ${}^oe_3^a {}^oe_2^b F_{ab}$ using the loop \square_{32} constructed from the composition of the following four segments:

- Segment 1: move from $(0, \pi/2, 0)$ to $(0, \pi/2, \lambda\ell_o)$ along the integral curve of ${}^oe_3 = \partial/\partial\gamma$;
- Segment 2: move along $(0, \pi/2, \lambda\ell_o)$ to $(\lambda\ell_o, \pi/2, \lambda\ell_o)$ along the integral curve of $-\xi_3^a = \partial/\partial\alpha$;
- Segment 3: move from $(\lambda\ell_o, \pi/2, \lambda\ell_o)$ to $(\lambda\ell_o, \pi/2, 0)$ along the integral curve of $-{}^oe_3 = -\partial/\partial\gamma$;
- Segment 4: return from $(\lambda\ell_o, \pi/2, 0)$ to the point of departure $(0, \pi/2, 0)$ along the integral curve of $\xi_3^a = -\partial/\partial\alpha$.

It is straightforward to calculate the holonomies along these four segments. One obtains

$$h_1 = e^{\lambda c \tau_3}, \quad h_2 = e^{-\lambda c (\sin \lambda \tau_1 + \cos \lambda \tau_2)}, \quad h_3 = e^{-\lambda c \tau_3} \quad h_4 = e^{\lambda \tau_2} \quad (\text{A14})$$

The holonomy $h_{\square_{32}}$ around the loop is just the composition $h_4 h_3 h_2 h_1$. A simple calculation yields:

$${}^oe_3^a {}^oe_2^b F_{ab}^k = \lim_{\lambda \rightarrow 0} \frac{4}{\lambda^2 \ell_o^2} \text{Tr}(h_{\square_{32}} \tau^k) = -\frac{1}{\ell_o^2} (c^2 - c\ell_o) \delta_1^k \quad (\text{A15})$$

Finally, using isotropy and homogeneity, one concludes:

$$\begin{aligned} F_{ab}^k &= -\lim_{\lambda \rightarrow 0} \frac{1}{\lambda^2 \ell_o^2} (\text{Tr } h_{\square_{ij}} \tau^k) {}^o\omega_a^i {}^o\omega_b^j \\ &= -\lim_{\lambda \rightarrow 0} \frac{1}{\lambda^2 \ell_o^2} [\sin^2 \lambda (c - \ell_o/2) - \sin^2(\lambda \ell_o/2)] \epsilon_{ij}^k {}^o\omega_a^i {}^o\omega_b^j \\ &= \ell_o^{-2} (c^2 - c\ell_o) \epsilon_{ij}^k {}^o\omega_a^i {}^o\omega_b^j \end{aligned} \quad (\text{A16})$$

The expression of the holonomy in the second step is used in the discussion of the Hamiltonian constraint in section II of the main text.

-
- [1] A. Ashtekar, T. Pawłowski and P. Singh, Quantum nature of the big bang, Phys. Rev. Lett. **96**, 141301 (2006), [arXiv:gr-qc/0602086](#).
 - [2] A. Ashtekar, T. Pawłowski and P. Singh, Quantum nature of the big bang: An analytical and numerical investigation I, Phys. Rev. **D73**, 124038, [arXiv:gr-qc/0604013](#).
 - [3] A. Ashtekar, T. Pawłowski and P. Singh, Quantum nature of the big bang: Improved dynamics, Phys. Rev. **D74**, 084003, [arXiv:gr-qc/0607039](#).
 - [4] C. Rovelli, Graviton propagator from background-independent quantum gravity, Phys. Rev. Lett. **97**, 151301 (2006), [arXiv:gr-qc/0508124](#);
E. Bianchi, L. Modesto, C. Rovelli, S. Speziale, Graviton propagator in loop quantum gravity, Class. Quantum Grav. **23**, 6989-7028 (2006), [arXiv:gr-qc/0604044](#);
E. R. Livine and S. Speziale, Group Integral Techniques for the Spinfoam Graviton Propagator, [arXiv:gr-qc/0608131](#).

- [5] M. Bojowald, Homogeneous loop quantum cosmology, *Class. Quantum Grav.* **20**, 2595-2615 (2003), [arXiv:gr-qc/0303073](#)
M. Bojowald, G. Date and K. Vandersloot, Homogeneous loop quantum cosmology: The role of the spin connection, *Class. Quantum Grav.* **21**, 1253-1278 (2004), [arXiv:gr-qc/0311004](#).
- [6] D. Green and W. Unruh, Difficulties with recollapsing models in closed isotropic loop quantum cosmology, *Phys. Rev. D* **70**, 103502 (2004), [arXiv:gr-qc/04-0074](#).
- [7] M. Bojowald, Absence of singularity in loop quantum cosmology, *Phys. Rev. Lett.* **86**, 5227-5230 (2001), [arXiv:gr-qc/0102069](#), Isotropic loop quantum cosmology, *Class. Quantum Grav.* **19**, 2717-2741 (2002), [arXiv:gr-qc/0202077](#).
- [8] A. Ashtekar, M. Bojowald, J. Lewandowski, Mathematical structure of loop quantum cosmology, *Adv. Theo. Math. Phys.* **7**, 233-268 (2003), [gr-qc/0304074](#).
- [9] K. Noui, A. Perez, K. Vandersloot, On the Physical Hilbert Space of Loop Quantum Cosmology, *Phys. Rev. D* **71** (2005) 044025; [arXiv:gr-qc/0411039](#).
- [10] L. Szulc, W. Kaminski, J. Lewandowski, Closed FRW model in loop quantum cosmology, [arXiv:gr-qc/0612101](#).
- [11] P. Laguna, The shallow waters of the Big-Bang, [arXiv:gr-qc/0608117](#).
- [12] A. Ashtekar and J. Lewandowski, Background independent quantum gravity: A status report, *Class. Quant. Grav.* **21**, R53-R152 (2004), [arXiv:gr-qc/0404018](#).
- [13] A. Ashtekar and M. Bojowald, Quantum geometry and the Schwarzschild singularity, *Class. Quant. Grav.* **23** (2006) 391-411, [arXiv:gr-qc/0509075](#).
- [14] Thiemann, T. Anomaly-free formulation of non-perturbative, four-dimensional Lorentzian quantum gravity, *Phys. Lett. B* **380**, 257-264 (1996), [gr-qc/9606088](#),
Quantum spin dynamics (QSD), *Class. Quant. Grav.* **15** 839-873 (1998), [gr-qc/9606089](#),
QSD V : Quantum gravity as the natural regulator of matter quantum field theories, *Class. Quant. Grav.* **15**, 1281-1314 (1998), [gr-qc/9705019](#).
- [15] T. Thiemann, *Introduction to Modern Canonical Quantum General Relativity* (CUP, Cambridge, at press).
- [16] K. Vandersloot, On the Hamiltonian constraint of loop quantum cosmology, *Phys. Rev. D* **71** 103506 (2005), [gr-qc/0502082](#);
Ph.D. Dissertation, submitted to The Pennsylvania State University (2006).
- [17] A. Perez, On the regularization ambiguities in loop quantum gravity, *Phys. Rev. D* **73** (2006) 044007, [arXiv:gr-qc/0509118](#).
- [18] J. M. Velhinho, Comments on the kinematical structure of loop quantum cosmology, *Class. Quant. Grav.* **21** (2004) L109, [arXiv:gr-qc/0406008](#).
- [19] C. Kiefer, Wave packets in minisuperspace, *Phys. Rev. D* **38**, 1761-1772 (1988).
- [20] A. Ashtekar, *Lectures on non-perturbative canonical gravity*, Notes prepared in collaboration with R. S. Tate (World Scientific, Singapore, 1991), Chapter 10;
A. Ashtekar and R. S. Tate, An algebraic extension of Dirac quantization: Examples, *Jour. Math. Phys.* **35** 6434-6470 (1994).
- [21] D. Marolf, Refined algebraic quantization: Systems with a single constraint [arXiv:gr-qc/9508015](#);
Quantum observables and recollapsing dynamics, *Class. Quant. Grav.* **12** (1995) 1199-1220 [arXiv:gr-qc:9404053](#)
Observables and a Hilbert space for Bianchi IX, *Class. Quant. Grav.* **12** (1995) 1441-1454 [arXiv:gr-qc:9409049](#)
Almost ideal clocks in quantum cosmology: A brief derivation of time, *Class. Quant. Grav.*

- 12** (1995) 2469-2486 [arXiv:gr-qc:9412016](#).
- [22] J. Louko and C. Rovelli, Refined Algebraic Quantization in the oscillator representation of $SL(2, \mathbb{R})$, *J. Math. Phys.* **D41**, 132-155 (2000), [arXiv:gr-qc/9907004](#).
 - [23] J. B. Hartle and S. W. Hawking, Wave Function Of The Universe, *Phys. Rev. D* **28**, 2960 (1983).
 - [24] A. Gil, J. Segura, N. M. Temme, Computing solutions of the modified Bessel differential equation for imaginary orders and positive arguments, *ACM. Trans. Math. Soft.* **30**, 145 (2004);
Algorithm 831: Modified Bessel functions of imaginary order and positive argument, *ACM. Trans. Math. Soft.* **30** 159 (2004).
 - [25] A. Ashtekar and T. Schilling, Geometrical formulation of quantum mechanics, In: *On Einstein's path*, A. Harvery, ed (Springer-Verlag, New York, 1998); [arXiv:gr-qc/9706069](#).
T. Schilling, Geometry of quantum mechanics, Ph.D. Dissertation, Penn State (1996), <http://cgpg.gravity.psu.edu/archives/thesis/index.shtml>
 - [26] J. Willis, On the low energy ramifications and a mathematical extension of loop quantum gravity, Ph.D. Dissertation, The Pennsylvania State University (2004); A. Ashtekar, M. Bojowald and J. Willis, Corrections to Friedmann equations induced by quantum geometry, IGPG preprint (2004).
 - [27] M. Bojowald and A. Skirzewski, Effective equations of motion for quantum systems, *Rev. Math. Phys.* **18**, 713-746 (2006); [arXiv:math-ph/0511043](#).
 - [28] V. Taveras, IGPG preprint (2006).
 - [29] P. Singh, A. Toporensky, Big Crunch Avoidance in $k = 1$ Semi-Classical Loop Quantum Cosmology, *Phys. Rev. D* **69** (2004) 104008, [arXiv:gr-qc/0312110](#).
 - [30] J. Lidsey, D. J. Mulryne, N. J. Nunes, R. Tavakol, Oscillatory Universes in Loop Quantum Cosmology and Initial Conditions for Inflation, *Phys. Rev. D* **70** (2004) 063521, [arXiv:gr-qc/0406042](#).
 - [31] T. Pawłowski, Genericity of classical universes in $k = 1$ FRW loop quantum cosmology, (in preparation).